PERGAMON

Quaternary Science Reviews 20 (2001) 1935–1953

QG QSR

Precise two chronometer dating of Pleistocene travertine: The $^{230}Th/^{234}U$ and $^{226}Ra_{ex}/^{226}Ra(0)$ approach

Jost Eikenberg[a,*], Guido Vezzu[a], Irene Zumsteg[a], Sixto Bajo[a], Max Ruethi[a], Georg Wyssling[b]

[a] *Paul Scherrer Institute, CH-5232 Villigen (PSI), Switzerland*
[b] *Büro Wyssling AG, CH-8118 Pfaffhausen (ZH), Switzerland*

Received 23 March 2000; received in revised form 22 November 2000; accepted 8 January 2001

Abstract

In order to determine the geochemical evolution of a freshwater limestone cave system located in central Switzerland (Hell Grottoes at Baar/Zug,) young postglacial tufaceous limestone and travertine precipitates were investigated using the $^{230}Th/^{234}U$ ingrowth system. Additional analyses of further radionuclides within the ^{238}U decay chain, i.e. ^{226}Ra and ^{210}Pb, showed that the Th/U chronometer started with insignificant inherited ^{230}Th over the entire formation period of the travertine setting (i.e. $^{230}Th(0) = 0$). A contribution from detrital impurities with $^{230}Th/^{234}U$ in secular equilibrium could be precisely subtracted by applying isochron dating of cogenetic phases and recently formed travertine. The resulting precise $^{230}Th/^{234}U$ formation ages were found to be consistent with the geological stratigraphy and were furthermore used to demonstrate the applicability of the next geologically important chronometer in the ^{238}U-decay series, based on decay of excess ^{226}Ra normalized to the initial, i.e. $^{226}Ra_{ex}/^{226}Ra(0)$. This system is suitable for dating phases younger than 7000 yr when the correction of a detritus component increasingly limits the precision of the $^{230}Th/^{234}U$ chronometer. Analytical solutions of the coupled $^{234}U/^{230}Th/^{226}Ra$ radionuclide system predicted that the $^{226}Ra_{ex}/^{226}Ra(0)$ chronometer is independent of the actual ^{230}Th activity build up from decay of ^{234}U, if the systems starts with zero inherited $^{230}Th(0)$. The data set confirmed this hypothesis and showed furthermore that the initially incorporated ^{226}Ra excess must have remained almost uniform in all limestone over a period of at least 7000 yr, i.e. 4–5 half-lives of ^{226}Ra. This is concluded because (i) the $^{226}Ra_{ex}/^{226}Ra(0)$ ages agreed well with those derived from $^{230}Th/^{234}U$, (ii) all data plot within uncertainty on the $^{226}Ra_{ex}/^{226}Ra(0)$ decay curve and (iii) the atomic Ba/Ca ratio was found to be constant in the travertine material independent of the sample ages. Provided that such boundary conditions hold, $^{226}Ra_{ex}/^{226}Ra(0)$ should be applicable to materials which are suitable for $^{230}Th/^{234}U$ dating in sedimentology and oceanography, i.e. travertine, corals, phosphorites, etc., and should strongly support $^{230}Th/^{234}U$ for samples that have been formed a few thousand years ago.

1. Introduction

The travertine limestone caves ("*Höllgrotten*", *Engl. Hell Grottoes)* investigated in this study are located near Lucerne at Zug/Baar, Switzerland (Fig. 1). Up to now it has not been possible to develop a convincing model of the geological setting and evolution of the massive speleothem. The underlying sedimentary strata suggests that the freshwater calcite precipitations were formed during global warming in the Holocene, i.e. less than 10,000 yr ago and fresh precipitates show that the formation of travertine is still active. Previous attempts using the most suitable dating methods available (^{14}C radiocarbon method, pollen analyses) for such a young setting have failed, because the carbon isotope composition in the extremely small fractions of fossil organic residues is strongly disturbed by carbon of inorganic origin from precipitating calcite. Pollen analysis is also not applicable due to strong dissolution of organic matter. However, for geological systems which have been developed less than 300 kyr ago, radionuclides from the U and Th decay series may be used as chronometers, provided that fractionation processes, such as different solubility, cause activity disequilibrium between the different members ($^{238,234}U$, ^{230}Th, ^{226}Ra, etc.) in the waters where the precipitates are forming (Edwards et al., 1987; Burnett et al., 1988; Sturchio and Binz, 1988; Osmond and Ivanovich, 1992; Kaufman,

*Corresponding author. Tel.: +41-56-310-2111; fax: +41-56-310-2309.
E-mail address: eikenberg@psi.ch (J. Eikenberg).

0277-3791/01/$ - see front matter
PII: S0277-3791(01)00020-8

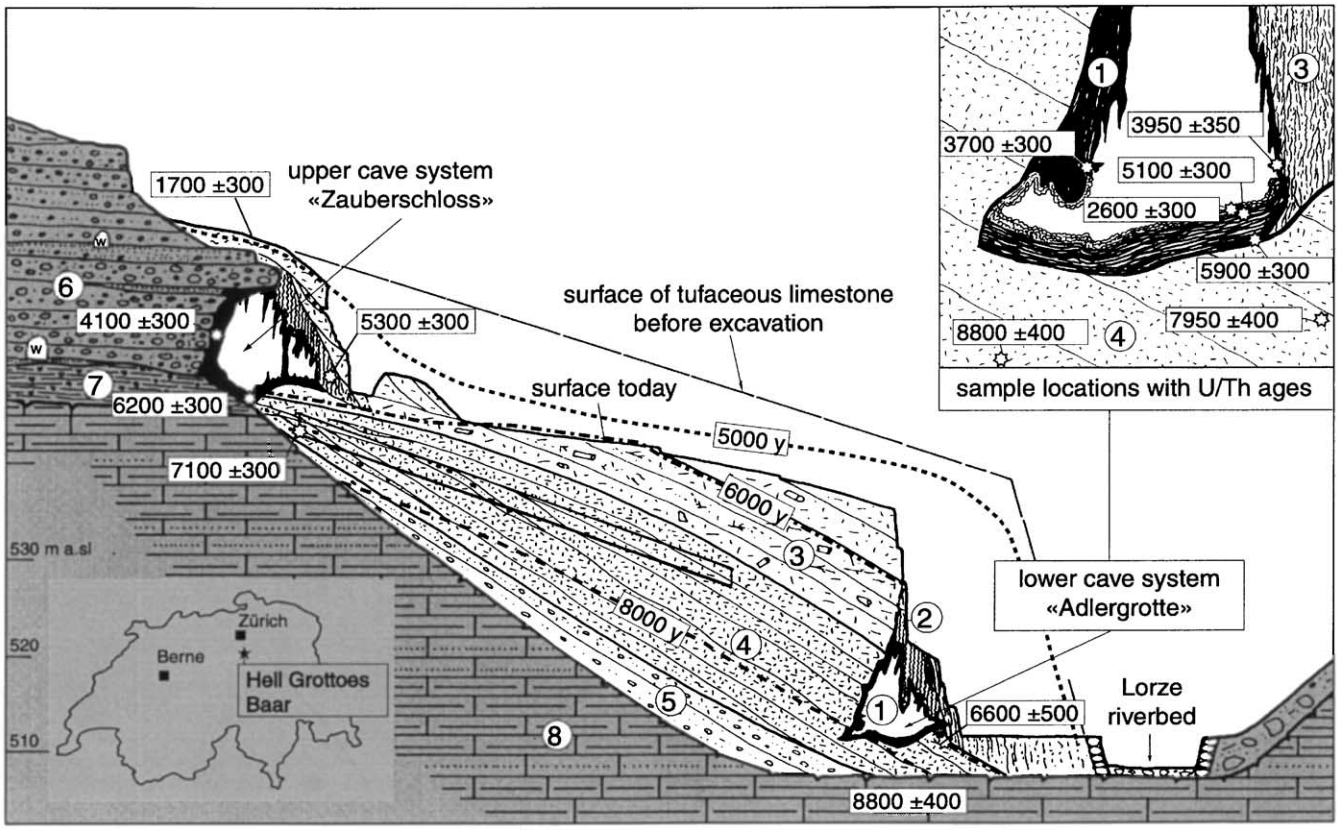

Fig. 1. Geological section through the limestone caves near Zug/Baar (Switzerland), The figure (scale ca. 100×50 m) distinguishes between 8 sedimentary formations (i) post-glacial formations: 1 = crystalline travertine, 2 = porous tufaceous limestone (tufcurtains), 3, 4 coarse and fine grained tufaceous limestone, 5 = talus deposits with tufaceous sand, (ii) glacial sediments: 6 = gravel with groundwater, 7 = moraine, (iii) pre-glacial sediments: 8 = upper freshwater molasse (marls and sandstone); w = drainage tunnel.

1993; Wagner, 1998). We therefore applied $^{230}Th/^{234}U$ ingrowth-dating on the travertine precipitates from this locality.

Since the isotope data indicated deposition of travertine in the Holocene, we also investigated the potential applicability of the next geologically important chronometer in the ^{238}U-decay series, based on decay of excess ^{226}Ra; $^{226}Ra_{ex}/^{226}Ra(0)$. Although $^{226}Ra_{ex}$ dating of speleothem has been rarely applied in the past, there are some interesting investigations suggesting that decay of excess inherited ^{226}Ra can be useful in obtaining formation ages and growth rates of Holocene sediments (i.e. Koide et al., 1976; Kim and Burnett, 1985; Latham et al., 1986; Sturchio, 1990; Latham and Schwarcz, 1992). While $^{230}Th/^{234}U$ ingrowth-dating covers a time span from about 4–300 kyr (where the system reaches secular equilibrium), ^{226}Ra excess-dating ($T_{1/2} = 1600$ yr) is ideal to investigate younger samples ranging from a few hundred years to about 7–8 kyr (or up to 5 half-lives). $^{226}Ra_{ex}$ chronometry is thus potentially a good complementary tool to support $^{230}Th/^{234}U$. However, three major requirements have to be fulfilled in order that $^{226}Ra_{ex}$ dating yields reliable results: (i) correct subtraction of a detrital, non-authigenic component, (ii) insignificant inherited, unsupported $^{230}Th(0)$ in the precipitating authigenic material and (iii) a constant initial concentration of $^{226}Ra(0)$ in all samples independent on the time of system closure. This study therefore investigates these three boundary conditions, presents an analytical-numerical approach to calculate precise $^{226}Ra_{ex}/^{234}U$ ages and focuses on the geological interpretation of the growth history of the cave system investigated here.

2. Geology and hydrochemistry

2.1. Geological setting

The *Hell Grottoes* belong to the lower part of the *Lorze Valley*, which was covered by the Muota-Reuss glacier during the last glaciation. After melting of the ice, strong erosion exposed more than 300 m thickness of quaternary sediments such as tills and highly permeable gravel sequences and, in the region of the *Hell Grottoes* (at the bottom of the valley) additionally the underlying less permeable strata (*Upper Freshwater Molasse*). Springs here continuously discharge infil-

trated rain and groundwater at the contact between these sequences (Fig. 1). Throughout the Holocene a tufaceous limestone-complex with a volume of about 200,000 m^3 (Heim, 1919) was built up. The deposit was mined for the production of brick stone during the 19th century (cf. Fig. 1 old and present day surface) until large caves were discovered and the mining was stopped in order to preserve the cave system. The freshwater precipitates consist mainly of porous tufaceous limestone that formed at the surface, assisted by assimilating plants (moss, algae). In the overhanging cliffs finely structured tuffcurtains were built up around tree roots and moss garlands, leading to the formation of the caves. As soon as the caves were closed by further growth of tuffcurtains, massive crystalline travertine precipitations coated the caves inside. Some of the caves were completely sealed by these precipitations which led to formation of lakes inside (Wyssling and Eikenberg, 2000).

2.2. Calcite precipitation

The limestone complex was formed via decomposition of organic matter in the soil by oxygen consuming bacteria causing increase in CO_2 as can be summarized by the simplified reaction

$$H_2CO + O_2 \rightarrow CO_2 + H_2O. \quad (1)$$

If the groundwater table is covered with less transmissive sediment or soil layers that derived from till, only fractions of carbon dioxide can escape to the atmosphere leading to a partial conversion via hydrolysis into hydrogen bicarbonate and dissolution of calcite (Krauskopf, 1979). When the groundwater, supersaturated with respect to pCO_2, discharges again on surface, CO_2 equilibrates with the atmosphere and is partially released as indicated by the following equation:

$$2HCO_3^- + Ca^{2+} \leftrightarrow CaCO_3 \downarrow + CO_2 \uparrow + H_2O. \quad (2)$$

With release of CO_2 the bulk reaction is shifted to the right side, which causes precipitation of calcite. While plants such as moss, shrub and tree roots are acting as crystallisation seeds for large amounts of carbonate precipitation on the surface, the rate of crystallization of pure travertine inside the caves is much slower because of the higher partial pressure of CO_2 in a semi-open system (Eq. 2).

3. Analytical methods

3.1. Sampling strategy

A compilation of the samples analyzed is presented in Table 1. The sampling strategy included the following considerations: (a) sampling of recently formed precipitations to obtain the initial value for $^{226}Ra(0)$, the maximum amount of inherited, not-supported $^{230}Th(0)$, and the variability of the U/Th ratio in the present day detritic, i.e. non-authigenic impurities; (b) sampling along profiles to check on the consistency of the isotope ages with the strata and to obtain growth rates; (c) sampling of co-genetically formed limestone to check on the reproducibility of the isotope ages and U/Th

Table 1
Geological characterisation of the travertine samples from the Hell Grottoes (Switzerland). A detailed explanation of the sampling strategy (items a–d) is given in the text

Sample #	Sample strategy	Geological and mineralogical description	$^{230}Th/^{234}U$ age (kyr)
1	(b)	Fine grained calcite tuff from the bottom of the deposit (profile I)	8.8 ± 0.4
2	(b)	Fine laminated, light brownish travertine on top of profile II	2.6 ± 0.3
3	(a)	Recent precipitations strongly intergrown with detrital clay minerals	<1
4	(b, c)	Brownish travertine crust from the surface of a small palaeolake	3.7 ± 0.3
5	(b, c)	Cogenetic aliquot of #4 from the other side of the palaeolake	3.9 ± 0.3
6	(d)	Fine grained, tufaceous limestone with inclusions of sandy tuff grains	7.1 ± 0.4
7	(b)	Porous calcite tuff on top of the lower cave system (profile I)	5.3 ± 0.3
8	(d)	Massive travertine from a level close to type 4, 5 samples	4.1 ± 0.3
9	(b)	Sample from the upper layer of the fine laminated limestone(profile I)	6.2 ± 0.4
10/1 + 2	(a, c)	Recent precipitations from a spring outside the caves (two aliquots)	0.5 ± 0.4
11	(b)	Travertine from a massive flowstone layer (profile II)	5.1 ± 0.3
12	(b)	Travertine from the bottom of a massive flowstone layer (profile II)	5.9 ± 0.3
13	(b)	Fine grained tufaceous limestone on the basement of profile I	7.9 ± 0.4
14/1 + 2	(c)	Two cogenetic porous tuffs from a wall of a cave outside the deposit	6.5 ± 0.5
14/3	(c)	Snail embedded in formation containing #14 (cogenetic aliquot)	6.6 ± 0.3
15	(d)	Purple travertine crystals on the surface of samples of type 4 + 5	3.5 ± 0.3
16	(d)	Massive stalagmites (re-crystallised travertine of the first generation)	7.1 ± 0.4
17	(d)	Fine laminated massive light brownish travertine	2.2 ± 0.3
18	(a)	young carbonate crusts (white, thin plates) outside the cave	1.7 ± 0.3
19	(a)	Very young calcite crust on the surface of a 10 y old electric wire	<0.4

composition of older detrital impurities via isochron straight lines, and (d) sampling of further selected material to specifically investigate the geological evolution of the cavern system at the particular study area. The assignment of the corresponding samples to items (a–d) is given in Table 1.

3.2. Sample preparation

Because of the very low radionuclide concentrations (typically between 0.3 and 10 mBq/g) samples of about 40 g were homogenized to fine grained powders with grain size $<200\,\mu m$. While one aliquot of 10 g was set aside for analysis of (volatile) ^{210}Po, another aliquot of 15 g was first heated to 500°C for 2 h (to destroy traces of organic components which reduce the chemical recoveries) and then split into two aliquots: 5 g for U/Th isotope analysis and 10 g for determination of ^{226}Ra via ^{222}Rn emanation (see below). To avoid isotope disturbances caused by infiltration of recent (acid) rainwater into the upper layers of the travertine caves (dissolution–re-deposition), all sample surfaces were cleaned by abrasion of a layer of a few mm thickness. However, some of the very fine grained tufaceous limestone samples which could not be abraded mechanically exhibited a significant excess of ^{210}Po compared to the progenitor nuclide ^{226}Ra, probably due to surface complexation of ^{210}Po and/or ^{210}Pb on co-precipitated organic matter. Such sample material is not suitable when using ^{210}Po as a measure of ^{226}Ra and other methods, such as direct measurement of ^{226}Ra or of its short-lived daughter ^{222}Rn (via the emanation method), have to be applied. In addition to the rock specimens, samples of the corresponding groundwater responsible for the carbonate precipitations were taken and analyzed for radionuclide concentrations as well as bulk chemical composition.

3.3. Analytical techniques

Rock samples: After complete sample dissolution in HNO_3 and addition of the chemical yield calibration spikes (^{232}U, ^{228}Th, ^{209}Po) the following nuclides were analyzed mainly using α-spectrometry: ^{238}U, ^{234}U, ^{232}Th, ^{230}Th and ^{226}Ra (the latter via its short-lived progenies ^{222}Rn and ^{210}Po). U and Th were separated chromatographically and consecutively on one column using UTEVA resin (Horwitz et al., 1993) produced by EiChroM Inc., Darien, USA, and the sample discs were prepared via electrolytic deposition using $HNaSO_4$–Na_2SO_4 buffer solution (Bajo and Eikenberg, 1999). ^{226}Ra was determined indirectly via its short-lived daughter ^{210}Po because the radioassay of Po is simple and yields highly precise results. The separation of Po was as follows: precipitation of Fe-hydroxide with NH_4OH, dissolution of the precipitate in 1 M HCl, in the presence of ascorbic acid to prevent deposition of Fe. Po was then separated via spontaneous deposition on silver discs. Radioassay of all these planar sources was performed using ultra-low-level high-resolution (16 keV) semiconductive surface barrier detectors (system Octete, Ortec Inc., USA). While ^{210}Po could be taken as a measure for ^{226}Ra for samples >100 yr, i.e. 5 half-lives of ^{210}Pb, all other samples, which could have been formed more recently, were also analyzed utilizing emanation of ^{222}Rn into an organic cocktail. Counting of organically bound ^{222}Rn and its very short-lived progenies ^{218}Po and ^{214}Po was then carried out under optimized settings for α/β discrimination, background scatter and counting efficiency (Eikenberg et al., 1999) using low level α/β-LSC (LS-counter, TriCarb 2550 TR/LL, Packard SA, Meriden, CT, USA).

Water samples: In freshwater ^{226}Ra and its progenies ^{210}Pb and ^{210}Po are likely to be in a state of disequilibrium, due to several sources and sinks for ^{210}Po and its geochemical relevant progenitors ^{210}Pb, ^{222}Rn and ^{226}Ra (Harada et al., 1989, Plater et al., 1995, Eikenberg et al., 2001a). Therefore it was essential to analyze ^{226}Ra directly, which was done similarly to the procedure given by Moore et al. (1995) via sorption of Ra on MnO_2. After sampling, the 1 l water samples were set aside for about 2 weeks to allow unsupported ^{224}Ra to decay and were then spiked using $^{228}Ra/^{224}Ra$ tracer solution to obtain the chemical yield precisely. Following the spiking each sample was exposed to MnO_2-coated polyvinyl discs for about 2 days and, thereafter, analyzed directly using α-spectrometry (detailed procedure in Eikenberg et al., 2001b).

In addition to the radioanalytical investigations, bulk chemical analyses were carried out applying ICP-MS and AAS (cations) and ion chromatography (anions). These investigations yielded the concentrations of all major and some minor stable elements in the carbonates as well as the waters (Ba, Sr, Ca, etc.).

4. Theory of $^{226}Ra/^{230}Th/^{234}U$ dating

Reducing the complex ^{238}U decay series into geologically relevant subsystems (i.e. nuclides with half-lives greater than a few years) the following precursor–progeny relations hold

$$^{238}U \rightarrow ^{234}U \rightarrow ^{230}Th \rightarrow ^{226}Ra\left(^{222}Rn\right) \rightarrow ^{210}Pb\left(^{210}Po\right), \quad (3)$$

where the nuclides in brackets tend rapidly towards secular equilibrium with their progenitors ($^{222}Rn \approx 3$ weeks, $^{210}Po \approx 1$ yr) and hence can be used as a measure of the activity of their parent nuclides. So far, two methods using mother/daughter relationships within the ^{238}U decay chain are mainly applied in the fields of

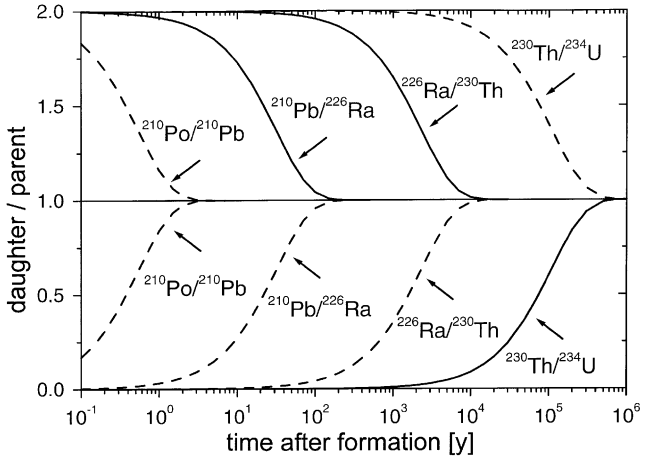

Fig. 2. Schematic illustration of time scales over which different pairs of the ^{238}U decay series members decay towards secular radioactive equilibrium (after Williams, 1987).

sedimentology and oceanography (i) ^{230}Th/^{234}U in-growth-dating for systems which evolved between 10 and 300 kyr (Edwards et al., 1987; Bischoff et al., 1988; Burnett et al., 1988; Bischoff and Fitzpatrick, 1991; Luo and Ku, 1991; Kaufman, 1993, etc.) and (ii) ^{210}Pb excess-decay dating (supplied from decay of soil-emanated ^{222}Rn into the atmosphere). The latter method is used mainly to determine sedimentation rates in lakes for sample ages of up to about 100 yr (Oldfield et al., 1978; Robbins, 1978). The third geologically meaningful chronometer which uses the decay of excess ^{226}Ra has been applied much more rarely because this method has to consider various boundary conditions (e.g. Koide et al. 1976; Kim and Burnett, 1985; Latham et al., 1986; Sturchio, 1990). However, this chronometer fills the time gap between the two more established chronometers and is suitable for dating between $\approx$ 100 yr and about 7–8 kyr or 5 half-lives of ^{226}Ra. This situation is illustrated in Fig. 2 which shows the evolution of the activity ratios in the ^{238}U series for hypothetical cases with initial daughter/parent ratios of 2 (twice daughter excess) and 0 (i.e. zero inherited daughter activity at the time of formation). The bold lines in Fig. 2 indicate all three chronometers of relevance in natural terrestrial systems while the dashed lines display all other hypothetical chronometers between the different members in the ^{238}U series.

In the following we present a detailed analytical approach for the coupled parent daughter system ^{226}Ra/^{230}Th/^{234}U/^{238}U. A complex analytical solution for ^{230}Th/^{234}U/^{238}U was first presented by Kaufman and Broecker (1965) who showed that, due to an unknown ^{234}U/^{238}U initial, ^{230}Th/^{234}U ages have to be obtained iteratively. However, for systems in which the ^{234}U/^{238}U activity ratios are close to unity (i.e. secular equilibrium), decay of ^{234}U depends on decay of the long lived parent ^{238}U or

$$^{234}\mathrm{U}(t) = {}^{234}\mathrm{U}(0)\mathrm{e}^{-\lambda_{238}t}, \quad (4)$$

where λ_{238} is the decay constant of the parent ^{238}U. Since decay of ^{238}U proceeds extremely slowly ($T_{1/2} = 4.5 \times 10^9$ yr) the activity of ^{234}U (supported from ^{238}U) remains almost constant in samples which formed less than a few 10 million years ago. Furthermore, if, the sample material is as young as a few thousand years, decay of slight excess of ^{234}U ($T_{1/2} = 2.5 \times 10^5$ yr) can also be disregarded. Given this situation, the activity of the next geologically relevant daughter, ^{230}Th, is not dependent on a change in ^{234}U, i.e.

$$^{230}\mathrm{Th}(t) = {}^{230}\mathrm{Th}(0)\mathrm{e}^{-\lambda_{230}t} + {}^{234}\mathrm{U}(1 - \mathrm{e}^{-\lambda_{230}t}). \quad (5)$$

While the first term on the righthand side of Eq. (5) refers to the decay of an initially inherited component of ^{230}Th, the second term describes the ingrowth of ^{230}Th in a mineral incorporating uranium. For samples starting without significant inherited ^{230}Th, the first term in Eq. (5) can be neglected, i.e. yielding the boundary condition $^{230}\mathrm{Th}(t=0)=0$. As noted above for young minerals <10 kyr with ^{234}U^{238}U a second boundary conditions holds, i.e. $^{234}\mathrm{U}(t) = {}^{234}\mathrm{U}(0)$. This is of advantage for calculating the evolution of the next daughter, ^{226}Ra, with time. The complex decay system involving ^{234}U, ^{230}Th and ^{226}Ra was solved using the computer program *MAPLE 5* (Radfern, 1996) and, the following analytical relation was obtained (neglecting 2nd order of the erms $1/\lambda_{230}$ and $1/\lambda_{238}$):

$$^{226}\mathrm{Ra}(t) = {}^{226}\mathrm{Ra}(0)\mathrm{e}^{-\lambda_{226}t} + {}^{234}\mathrm{U}\frac{\lambda_{226}(1 - \mathrm{e}^{-\lambda_{230}t}) - \lambda_{230}(1 - \mathrm{e}^{-\lambda_{226}t})}{\lambda_{226} - \lambda_{230}}, \quad (6)$$

where, as above, the first term refers to decay of initially incorporated ^{226}Ra, while the second describes the delayed ingrowth of ^{226}Ra via ingrowth of ^{230}Th. Provided that the boundary conditions given above are fulfilled, these relations show clearly that the ^{230}Th ingrowth is dependent only on ^{234}U and, therefore, the ^{230}Th supported ^{226}Ra ingrowth is also dependent on the activity of ^{234}U alone. Hence under such ideal conditions we can conclude that for this coupled system there is no need to determine ^{230}Th analytically, this couple can be referred as $^{226}\mathrm{Ra}_{ex}/^{234}$U chronometer or (as shown below) normalized to initial radium as $^{226}\mathrm{Ra}_{ex}/^{226}\mathrm{Ra}(0)$. The ^{230}Th/^{234}U and $^{226}\mathrm{Ra}_{ex}/^{234}$U ingrowth relationships are shown theoretically in Fig. 3 for an ideal system which started under the boundary conditions defined above, and for three different initial $(^{226}\mathrm{Ra}_{ex}/^{234}\mathrm{U})_0$ activity ratios of 0.2, 0.5 and 1.

5. Results and discussion

The results of the U and Th isotope analysis are presented, in terms of their activities, in Table 2. The typical relative uncertainties (in 2σ) are ^{234}U, ^{238}U: 1–3%, $^{234}U/^{238}U$: 2–5%, ^{230}Th: 4–10%, ^{232}Th for samples with $^{234}U/^{232}Th$ activity ratios of ≈ 100, about 10–30%. While the activities of the U-isotopes are fairly constant in the travertine samples, ^{230}Th is more variable because of different sample ages and/or contribution of a detrital component also containing ^{232}Th and ^{238}U with all progenies in secular equilibrium (see discussion below). In an average sample (for instance #4, 5, 8) the activities of ^{230}Th are very low (≈ 0.2 mBq/g or $\approx 3 \times 10^{-15}$ mol/g. For this reason all samples were counted for about one week. The activities of ^{210}Po and ^{222}Rn are given in Table 3 along with a compilation of the $^{230}Th/^{234}U$ and $^{226}Ra_{ex}/^{226}Ra(0)$ ages and the results of the bulk chemical investigations are summarized in Table 4 including the results for ^{226}Ra in the water sample.

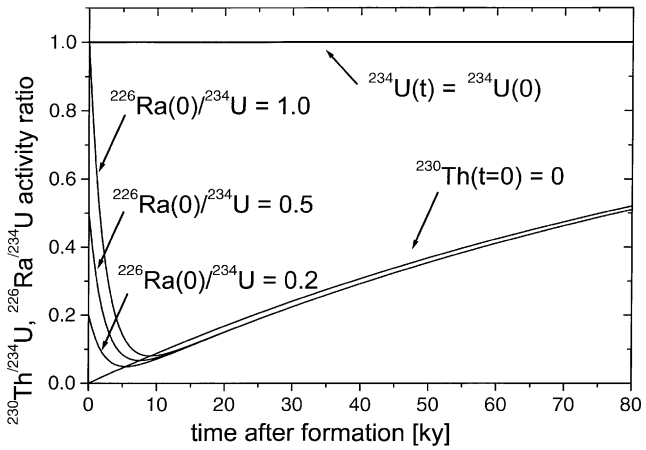

Fig. 3. Theoretical parent/daughter ingrowth/decay relationships for the chronometers $^{230}Th/^{234}U$ and $^{226}Ra_{ex}/^{234}U$ as a function of time for systems starting without initial ^{230}Th and for three sets of initial $^{226}Ra_{ex}/^{234}U$ activity ratios of 0.2, 0.5 and 1.0.

5.1. Dating with the $^{230}Th/^{234}U$ chronometer

5.1.1. Correction for non-authigenic (detrital) material

One of the major requirements for correct use of the $^{230}Th/^{234}U$ chronometer on a single sample is knowledge of the initial activity values at the time when the system's clock started. In the case of limestone precipitations there is a further complication because the freshly precipitating, authigenic phases are generally intergrown to a certain degree with detrital material (mainly clays) containing U and Th of different age. However, as discussed in a compilation given by Kaufman (1993) it is reasonable to assume that such material is older than a few 100 kyr, i.e. all members within the U and Th decay series are in or close to secular equilibrium ($^{234}U = {}^{230}Th = {}^{226}Ra$). This means that independent of the degree of the detrital impurities, internal isochrons

Table 2
Results of the U and Th isotope analysis and calculated ($^{230}Th/^{234}U$) ratios in the authigenic, pure carbonates

#	^{238}U (mBq/g)	^{234}U (mBq/g)	^{230}Th (mBq/g)	^{232}Th (mBq/g)	$\left(\frac{^{234}U}{^{232}Th}\right)_m$	$\left(\frac{^{230}Th}{^{232}Th}\right)_m$	$\left(\frac{^{234}U}{^{238}U}\right)_{aut}$	$\left(\frac{^{230}Th}{^{234}U}\right)_{aut}$
1	4.04	5.33	0.46	0.04	133	11.5	1.32	0.077
2	4.45	5.58	0.18	0.04	140	4.5	1.26	0.023
3	4.40	5.48	1.27	0.97	5.65	1.3	1.34	<0.01
4	4.30	5.29	0.20	0.02	265	10.0	1.23	0.033
5	5.62	6.69	0.26	0.02	335	12.9	1.19	0.035
6	5.68	7.44	0.58	0.09	82.7	6.4	1.31	0.063
7	7.97	10.3	0.65	0.13	79.2	5.0	1.30	0.047
8	3.82	4.99	0.21	0.02	250	10.5	1.31	0.037
9	4.54	5.92	0.45	0.10	59.2	4.5	1.31	0.055
10/1	3.13	4.04	0.38	0.28	14.4	1.4	1.33	0.004
10/2	3.16	3.94	0.40	0.30	13.1	1.3	1.28	0.005
11	5.53	7.09	0.34	0.01	709	34.0	1.28	0.046
12	9.45	12.2	0.66	0.02	816	43.9	1.30	0.052
13	6.67	8.41	0.64	0.04	205	15.6	1.26	0.070
14/1	3.01	3.83	0.48	0.21	18.2	2.3	1.30	0.058
14/2	6.75	8.62	0.56	0.02	431	28.0	1.28	0.062
14/3	19.3	24.8	1.54	0.06	413	25.7	1.29	0.059
15	4.16	5.14	0.18	0.01	509	17.8	1.24	0.033
16	13.5	17.1	1.09	0.01	1750	109	1.26	0.064
17	4.20	5.16	0.14	0.03	172	4.7	1.23	0.020
18	5.08	6.21	0.11	0.01	621	11.0	1.22	0.016
19	6.60	8.65	0.04	0.03	228	1.3	1.31	<0.002
gw[a]	13.0	16.5	<0.01	<0.01	>1000		1.27	<0.001

[a] gw = present day groundwater.

Table 3
Measured ^{210}Po and ^{222}Rn activities as well as calculated activities of the components $^{226}Ra_{aut}$ and $^{226}Ra_{ex}$. A comparison of $^{230}Th/^{234}U$ and $^{226}Ra_{ex}/^{226}Ra(0)$ formation ages is also presented[a]

#	$^{210}Po_m$ (mBq/g)	$^{222}Rn_m$ (mBq/g)	$^{226}Ra_{aut}$ (mBq/g)	$^{226}Ra_{ex}$ (mBq/g)	$^{230}Th/^{234}U$ age (kyr)	$^{226}Ra_{ex}/^{226}Ra(0)$ age (kyr)
1	0.38 ± 0.02		0.33 ± 0.02	0.02 ± 0.03	8.8 ± 0.4	> 7
2	0.39 ± 0.02	0.38 ± 0.07	0.34 ± 0.03	0.29 ± 0.03	2.6 ± 0.3	3.0 ± 0.3
4	0.31 ± 0.02	0.33 ± 0.07	0.28 ± 0.02	0.19 ± 0.02	3.7 ± 0.3	3.9 ± 0.4
5	0.34 ± 0.02	0.29 ± 0.07	0.31 ± 0.02	0.19 ± 0.02	3.9 ± 0.3	3.9 ± 0.4
6	0.47 ± 0.03	n.a.	0.35 ± 0.03	0.03 ± 0.04	7.1 ± 0.4	> 7
7	6.82 ± 0.15	0.63 ± 0.11	6.65 ± 0.15	6.35 ± 0.18	5.3 ± 0.3	(a)
8	0.35 ± 0.02	n.a.	0.32 ± 0.02	0.23 ± 0.03	4.1 ± 0.3	3.6 ± 0.5
9	0.43 ± 0.02	n.a.	0.30 ± 0.03	0.08 ± 0.04	6.2 ± 0.4	5.8 ± 2.7
10	1.13 ± 0.04	1.19 ± 0.15	0.77 ± 0.04	0.76 ± 0.04	0.5 ± 0.4	0.7 ± 0.1
11	0.33 ± 0.02	n.a.	0.32 ± 0.02	0.12 ± 0.03	5.1 ± 0.3	5.0 ± 2.0
12	0.52 ± 0.03	n.a.	0.50 ± 0.03	0.09 ± 0.04	5.9 ± 0.3	5.8 ± 2.5
13	0.54 ± 0.03	n.a.	0.49 ± 0.03	0.06 ± 0.04	7.9 ± 0.4	6.5 ± 4.2
14/1	0.53 ± 0.03	0.60 ± 0.11	0.26 ± 0.04	0.11 ± 0.04	6.5 ± 0.5	5.3 ± 1.9
15	0.40 ± 0.02	n.a.	0.39 ± 0.02	0.31 ± 0.03	3.5 ± 0.3	2.8 ± 0.3
16	0.77 ± 0.03	n.a.	0.76 ± 0.03	0.01 ± 0.04	7.1 ± 0.4	> 7
17	0.40 ± 0.02	n.a.	0.36 ± 0.02	0.32 ± 0.02	2.2 ± 0.3	2.7 ± 0.2
18	0.48 ± 0.03	n.a.	0.47 ± 0.03	0.44 ± 0.03	1.7 ± 0.3	2.0 ± 0.2
19	2.41 ± 0.08	1.11 ± 0.14	1.05 ± 0.12	1.05 ± 0.12	< 0.4	< 0.1

[a] n.a. = not analyzed, (a) not determined due to surface contamination with excess ^{210}Po.

Table 4
Bulk chemical compositions of six travertine samples and present day groundwater

Element (mg/g)	Sample #(in sequence with increasing U/Th-age) (mg/g)						
	#19	#10	#2	#4	#12	#13	g.w.[a] (mg/l)
Na^+	0.39	0.41	0.41	0.38	0.40	0.42	3.73
K^+	0.05	0.11	0.05	0.07	0.06	0.09	0.54
Mg^{2+}	3.29	2.79	3.60	3.55	3.72	3.61	18.3
Ca^{2+}	399	380	396	392	397	385	142
Sr^{2+}	0.25	0.23	0.17	0.26	0.30	0.21	0.279
Ba^{2+}	0.19	0.19	0.18	0.19	0.19	0.18	0.089
Ra^{2+}[b]	3.0×10^{-11}	3.0×10^{-11}	1.1×10^{-11}	8.4×10^{-12}	1.4×10^{-11}	1.5×10^{-11}	1.8×10^{-11}
Zn^{2+}	0.03	0.03	0.03	0.02	0.03	0.02	0.041
SO_4^{2-}	4.05	3.75	4.35	3.82	3.90	3.97	3.38
Mg/Ca	8.2×10^{-3}	7.3×10^{-3}	9.1×10^{-3}	9.1×10^{-3}	9.4×10^{-3}	9.4×10^{-3}	1.3×10^{-1}
Sr/Ca	6.3×10^{-4}	6.1×10^{-4}	4.3×10^{-4}	6.6×10^{-4}	7.6×10^{-4}	5.5×10^{-4}	2.0×10^{-3}
Ba/Ca	4.8×10^{-4}	5.0×10^{-4}	4.6×10^{-4}	4.8×10^{-4}	4.8×10^{-4}	4.7×10^{-4}	6.3×10^{-4}
Ra/Ca	7.5×10^{-14}	7.9×10^{-14}	2.8×10^{-14}	2.1×10^{-14}	3.5×10^{-14}	3.9×10^{-14}	1.3×10^{-14}
Ra/Ba	1.6×10^{-10}	1.6×10^{-10}	6.1×10^{-11}	4.4×10^{-11}	7.4×10^{-11}	8.3×10^{-11}	2.0×10^{-10}

[a] g.w. = present day groundwater.
[b] calculated from radiochemical determination.

connecting all cogenetic phases can be written by normalizing the $^{230}Th/^{234}U$ decay/ingrowth relationship to ^{232}Th, or

$$\frac{^{230}Th(t)}{^{232}Th} = \frac{^{230}Th(0)}{^{232}Th} e^{-\lambda_{230} t} + \frac{^{234}U}{^{232}Th}(1 - e^{-\lambda_{230} t}), \quad (7)$$

where λ_{230} is the decay constant of ^{230}Th and the slope m (or the isochron $= 1 - e^{-\lambda} 230^t$) yields the age of all (cogenetic) samples which have been formed simultaneously. Basically, relation 7 is useful to distinguish between two mixed phases (e.g. travertine, detrital silicates) and therefore to eliminate the uncertainties on predominantly $^{230}Th(0)$. A thorough explanation of $^{230}Th/^{232}Th$–$^{234}U/^{232}Th$ isochron relationships, introduced first by Allègre and Condomines (1976), can be obtained from the reviews by Gill et al. (1992) or MacDougall (1995) and several successful demonstrations have been presented for dating authigenic sediments (Bischoff and Fitzpatrick, 1991; Luo and Ku, 1991; Kaufman, 1993; Israelson et al., 1997; Kaufman et al., 1998). A typical isochron relationship of the samples investigated here is shown in Fig. 4 for two simultaneously formed fine grained travertine from the bottom of the deposit (#14/1and 14/2) including a fossil

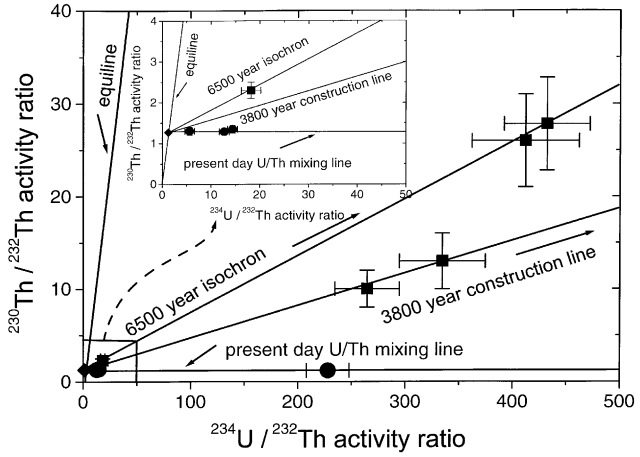

Fig. 4. ^{230}Th/^{232}Th - ^{234}U/^{232}Th isotope diagram showing isochrons connecting cogenetic travertine of different age (6.5 kyr, and present day U/Th mixing line obtained from recently formed limestone). Both regression lines intersect the equiline at ^{230}Th/^{232}Th and ^{234}U/^{232}Th = 1.3, indicating uniform U/Th ratios of the detrital component in all samples from the deposit The analytical uncertainties are given as 2σ.

snail (#14/3) which could be purified from the surrounding material of type #14. The isochron straight line intercepts with the equiline or the detrital component (i.e. the line on which all samples are in secular equilibrium or ^{230}Th/^{234}U = 1) at ^{230}Th/^{232}Th (or ^{234}U/^{232}Th) = 1.3 + 0.1. A second regression line in Fig. 4 connects the U/Th isotope data of two recently formed young precipitates taken from a spring outside the limestone caves, more (#3) or less (#10, two aliquots) strongly intergrown with detrital material, as well as very young travertine coatings (#19) overgrowing a 10 yr old electric wire. These zero age samples define the present day mixing line, which intersects the equiline at ^{230}Th/^{232}Th = 1.3 + 0.1. This horizontal line therefore documents (at least for recently formed limestone) a uniform ^{230}Th/^{232}Th ratio for the detrital component. In addition to this, another sequence of co-genetic phases was collected, that are two travertine samples taken from the same sea level of a paleolake, (#4 and 5). Clearly two samples are not sufficient for calculation of an isochron slope, but a construction line connecting these samples with the detrital ^{230}Th/^{232}Th ratio defined by the other co-genetic samples is, within error, consistent with the U/Th isotope ratios of #4 and 5.

It is, therefore, very likely that all travertine analyzed here contain detrital inclusions with identical ^{238}U/^{232}Th ratios because the three slopes cover a period in which most of the travertine was deposited (i.e. between present day and $\approx$ 9000 yr). Given this situation all other samples should be datable applying the ^{230}Th/^{234}U isotope pair without the need of constructing individual isochrons, i.e. via analysis of several cogenetic phases or sample leachates to obtain one single formation age. With a constant U/Th ratio in the detrital phase, correction for such impurities can be simply obtained via subtraction of ^{232}Th times the detrital U/Th ratio from measured $^{234}U_m$ and $^{230}Th_m$ or, for instance, for ^{234}U

$$^{234}U_{aut} = ^{234}U_m - k\,^{232}Th_m, \quad (8)$$

where k refers to the ^{234}U/^{232}Th ratio of the impure detritus and the subscript 'aut' refers to the ^{234}U activity in the pure, authigenic material. Following the detritus correction, the ^{230}Th/^{234}U age can be obtained simply by rearranging Eq. (5), i.e.

$$t_{age} = -\frac{1}{\lambda}\ln\left(1 - \frac{^{230}Th_{aut}}{^{234}U_{aut}}\right). \quad (9)$$

Since in addition for young systems <10 kyr the ^{234}U activity remains almost constant (decay of maximum 3% if not supported by ^{238}U), the equipoint can be directly used to extract the U/Th ratio of the detrital phases. Since ^{234}U/^{238}U = 1.3 for typical travertine (Table 1) like ^{230}Th/^{232}Th on the equipoint, a ^{238}U/^{232}Th activity ratio of 1.0 results for the detrital phase. Converted to more convenient mass units, this corresponds to a ^{232}Th/^{238}U mass ratio of 3 which is typical for crustal silicate rocks.

5.1.2. Maximum inherited initial $^{230}Th/^{234}U$ ratios in recently forming calcite

Eq. (9) does not contain any term relating to a component of inherited or excess (i.e. unsupported) ^{230}Th, or a change of the activity of $^{234}U_{aut}$ with time, as does Eq. (5). In the case of uranium, the samples are characterized by similar ^{234}U/^{238}U ratios of 1.28 + 0.04 (mean value of all data in Table 2) indicating rather low excesses of ^{234}U in comparison with ^{238}U. This means that for system closure times <10 kyr, the change in ^{234}U/^{238}U from decay of excess ^{234}U is extremely small (<1% for samples which crystallized 10 kyr ago). Since the change of the U-isotope activity ratio is still less for younger samples, it can be reasonably considered that the ^{234}U activity remained constant in all samples analyzed here.

The second assumption (^{230}Th(0) = 0) is somewhat more difficult to prove, because, although the solubility of Th^{4+} in aqueous solutions is orders of magnitude below that of UO_2^{2+} (Fuger and Oetting, 1976; Langmuir, 1978; Langmuir and Herman, 1980; OECD, 1992), there remains the possibility that ^{230}Th (from decay of dissolved ^{234}U) forms colloids or adsorbs on suspended matter as has been shown to be the most likely case for its presence in river and ground waters (Langmuir and Herman, 1980, Tricca, 1997). We therefore analyzed fresh groundwater from which travertine is continuously precipitating. Radioassay of this water including complete digestion of all particles in

$HF\text{-}HNO_3$ yielded no detectable activity of ^{230}Th as well as ^{232}Th ($<1\times10^{-5}$ Bq/l). Expressed in mass units these detection limits convert to: $^{230}Th<3\times10^{-14}$ g/l and $^{232}Th<3\times10^{-9}$ g/l, i.e. detection limits which do not exceed the values obtained from non-turbulent river waters and estuaries as reported, for instance, by Anderson et al. (1995) using high sensitivity thermal ion mass spectrometry (TIMS). In contrast to Th, a significant activity of U-isotopes ($^{234}U=16.5$ mBq/l) was measured, yielding an $^{230}Th/^{234}U$ activity ratio $<6\times10^{-4}$. Assuming conservatively that the co-precipitation yield for unsupported ^{230}Th exceeds that of ^{234}U by a factor of 10, the initial $(^{230}Th/^{234}U)_{aut}$ activity ratios in the recently formed limestone still remain $<6\times10^{-3}$, i.e. a value which is consistent to the $(^{230}Th/^{234}U)_{aut}$ activity ratios obtained for the recently formed travertine samples #10 and #19.

5.1.3. Maximum inherited initial $^{230}Th/^{234}U$ ratios in older samples

Thus, in summary, it can be concluded that the present day precipitates do not incorporate significant quantities of $^{230}Th(0)$, but how can one further prove that the present day water is chemically similar to its composition a few thousand years ago? To answer this question the $^{234}U/^{238}U$ ratios in the rock and water samples can be used, because independent of the precipitation yield of uranium in the individual samples, the $^{234}U/^{238}U$ ratio should remain constant in solid and aqueous phases if the limestone precipitated from one water source with uniform $^{234}U/^{238}U$. Fig. 5 shows that, within error, the U-isotope ratios of the rock samples remained constant at $1.28+0.06$ independent of the time of formation and that this value also agrees with the present day $^{234}U/^{238}U$ ratio in the corresponding groundwater (at $1.27+0.04$). The data therefore suggest that the precipitates are likely to have formed from a chemically similar water source, the more so, since the concentrations of stable elements such as Na^+ and, in particular, the bivalent ions , Mg^{2+}, Ba^{2+}, SO_4^{2-} in six samples analyzed here (Table 4, and Ba/Ca ratios in Fig. 5) are almost identical.

There are, in addition, two further points which support the assumption that the travertine investigated here did not incorporate significant amounts of inherited ^{230}Th. For samples >8 kyr more than 97% of initial ^{226}Ra excess has decayed, therefore ^{226}Ra and ^{230}Th should be in a fixed transient activity equilibrium. As will be shown below (discussion on Ra) this is indeed confirmed by comparison of the $^{226}Ra/^{230}Th$ data of such old samples to the theoretical value obtained when calculating with $^{230}Th(0)=0$.

The other point is that the $^{230}Th/^{234}U$ ages are consistent with the relative succession of the geological strata. The continuously increasing $^{230}Th/^{234}U$ formation ages with depth is indicated for two profiles through the tufaceous limestone outside and travertine flow stones inside the lower cave system (Table 5, Fig. 1). Table 5 shows that samples with variable initial $(^{230}Th/^{234}U)_{aut}$ in the order of 6×10^{-3} (which introduces an error of up to 1 kyr) are likely to violate the relative age sequence in the profile.

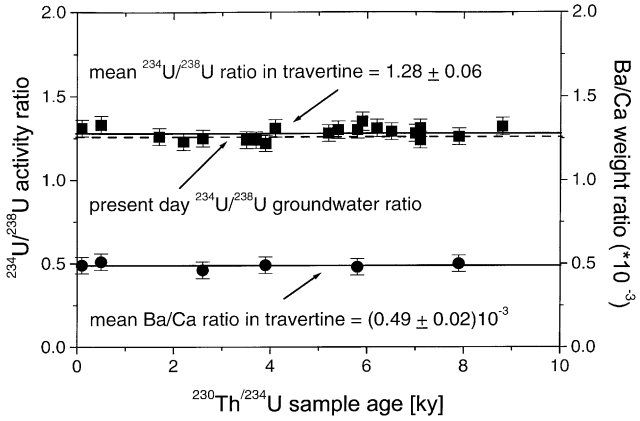

Fig. 5. Plot of the $^{234}U/^{238}U$ activity and Ba/Ca weight ratios of the travertine samples versus their $^{230}Th/^{234}U$ formation ages (uncertainties: 2σ). The dashed line indicates the U-isotope ratio for present day groundwater.

5.2. Dating with the $^{226}Ra_{ex}/^{226}Ra$ chronometer

5.2.1. Previous studies

In a similar manner to the $^{230}Th/^{234}U$ pair normalized to long-lived ^{232}Th, isochron dating using $^{226}Ra/^{230}Th$ was introduced by Williams et al. (1986) to investigate magma genesis and several applications in volcanology have been presented since (Williams, 1987; Condomines et al., 1988; Volpe and Hammond, 1991; Volpe, 1992; Volpe and Goldstein, 1993; Chabaux and Allègre et al., 1994). Since, beside ^{226}Ra, no long-lived Ra isotope can be found in nature, it was suggested to use stable Ba as normalization isotope because this element behaves chemically in an analogous manner to Ra. However if short-lived systems are considered, precise ages can be obtained by normalizing ^{228}Ra ($T_{1/2}=5.7$ yr) to ^{226}Ra. A good example of the applicability of $^{228}Ra_{ex}/^{226}Ra$ chronometry was presented by Sturchio (1990) who investigated the diagenetic transformation from aragonite to calcite at Mammoth Hot Spring, Wyoming. Due to the short half-life of ^{228}Ra this chronometer is suitable only for samples that formed less than 20–30 yr ago. For precipitations that formed a few thousand years ago further interesting examples can be found in the literature, demonstrating that non-normalized ^{226}Ra-excess dating may also yield meaningful ages. Applications were presented for marine sediments (Koide et al., 1976) or phosphorites (Kim and Burnett, 1985) as well as travertine and speleothem (Latham

Table 5
$^{230}Th/^{234}U$ ages of samples from profiles through the tufaceous limestone outside and travertine flow stones inside the lower cave system. The locations of 6 of the 8 samples from both profiles are also shown in the magnification of the lower cave system in Fig. 1

Profile I. Tufaceous limestone				Profile II. Travertine flow stone			
Sample #	$^{230}Th/^{234}U$ age (kyr)	Distance from bottom (cm)	Growth rate (cm/kyr)	Sample #	$^{230}Th/^{234}U$ age (kyr)	Distance from bottom (cm)	Growth rate (cm/kyr)
7	5.3 ± 0.3	550	60	2	2.6 ± 0.3	70	10
9	6.2 ± 0.4	350	120	4. 5	3.7 ± 0.3	60	15
13	7.9 ± 0.4	150	170	11	5.1 ± 0.3	40	50
1	8.8 ± 0.4	0		12	5.9 ± 0.3	0	

et al., 1986; Romano et al., 1987; Sturchio, 1990). The study of Latham et al. (1986) showed, for instance, good concordance between ^{14}C- and $^{226}Ra_{ex}$-ages in a Mexican stalagmite. Kim and Burnett (1985), however, measured in phosphate nodules from the Peru/Chile seafloor with U/Th ages > 10 kyr repeatedly $^{226}Ra/^{230}Th$ ratios below unity, speaking for removal of ^{226}Ra in rather old samples where both nuclides should be in transient equilibrium. While most of the investigations assume that ingrowth of ^{226}Ra from decay of ^{230}Th is not significant (and hence do not consider any corrections), Koide et al. (1976) discussed an approach to correct for ^{226}Ra supported from decay of ^{230}Th (however not considering dynamic ingrowth of ^{230}Th from ^{234}U). A detailed analytical solution of the complex system $^{238}U/^{234}U/^{230}Th/^{226}Ra$ was presented by Kim and Burnett (1985) who extended the analytical solution given by Kaufman and Broecker (1965) for the U/Th system to ^{226}Ra. In order to obtain $^{226}Ra_{ex}$-ages such complex solutions have to be solved iteratively. However, provided that the boundary conditions $^{230}Th(0) = 0$ and $^{234}U(t) = {}^{234}U(0)$ are correct, there is simple way to calculate precise $^{226}Ra_{ex}/^{234}U$ or $^{226}Ra_{ex}/^{226}Ra(0)$ ages considering changing activity concentrations of ^{226}Ra supported by ingrowth of ^{230}Th.

5.2.2. Correction for non-authigenic (detrital) material

After having shown that at least for the samples investigated here (i) detrital impurities can be subtracted using a constant U/Th ratio in that phase and that (ii) all samples started without significant amounts of inherited ^{230}Th, it is possible to apply the analytical solution for ingrowth and decay of ^{226}Ra, the third geochemically important radionuclide in the ^{238}U decay series. Since the second term in Eq. (6) describes the ^{230}Th supported ingrowth of ^{226}Ra ($^{226}Ra_{sup}$), the amount of the residual excesses of ^{226}Ra surviving the decay of initially incorporated Radium can be calculated as follows:

$$^{226}Ra_{ex}(t) = {}^{226}Ra_{aut} - {}^{226}Ra_{sup}(t), \quad (10)$$

where $^{226}Ra_{aut}$ is the total activity of ^{226}Ra in the pure authigenic phase. Assuming secular equilibrium between ^{230}Th and ^{226}Ra in the detrital phase yields, similar to Eq. (8)

$$^{226}Ra_{aut} = {}^{226}Ra_m - k^{232}Th_m. \quad (11)$$

5.2.3. Comparison of the $^{226}Ra_{aut}/^{234}U$ data with the $^{226}Ra_{ex}$-decay/$^{226}Ra_{sup}$-ingrowth relationship

Eq. (10) shows clearly that calculation of $^{226}Ra_{ex}(t)$ still requires knowledge of two components, $^{226}Ra_{aut}$ (which can be simply calculated by use of Eq. (11)) and $^{226}Ra_{sup}(t)$ from ingrowth of the precursor ^{230}Th. The evolution of $^{226}Ra_{sup}(t)$ normalized to ^{234}U is shown in Fig. 6 taking $^{226}Ra(0)/^{234}U$ from the most recently formed sample (#19, discussion next paragraph), as a fixed parameter. In contrast to Fig. 3 two more curves are presented in this figure, i.e. the decay of $^{226}Ra_{ex}$ and the ^{230}Th supported ingrowth of ^{226}Ra, i.e. $^{226}Ra_{sup}$. It is indicated that $^{226}Ra_{sup}$ is strongly delayed because at short times both terms, $\lambda_{230}(1-e^{-\lambda}230^t)$ and $\lambda_{226}(1-e^{-\lambda}226^t)$ in Eq. (6) yield very similar values, while with increasing life time of the system the term $\lambda_{226}(1-e^{-\lambda}226^t)$ tends more rapidly towards 1 than the ingrowth term of ^{230}Th. This leads to a transient, fixed equilibrium between $^{230}Th_{sup}$ and $^{226}Ra_{sup}$ tending to $\lambda_{226}/(\lambda_{226} - \lambda_{230}) = 1.02$ for $t \gg T_{1/2}$ (^{226}Ra).

It is now interesting to compare the measured $^{226}Ra_{aut}/^{234}U$ data with the $^{226}Ra(t)/^{234}U$ decay/ingrowth curve. To be able to do this, two parameters have to be known (i) the age of the samples obtained from an independent method, and (ii) the value for $^{226}Ra(0)/^{234}U$. While the sample ages were taken from the $^{230}Th/^{234}U$ chronometer, the initial $^{226}Ra(0)/^{234}U$ was obtained from the most recently formed sample (#19), in which there is a disequilibrium between ^{210}Po and ^{222}Rn (Table 2) and which must, therefore, be younger than 100 yr (c.f. Fig. 2, $^{210}Pb/^{226}Ra$ relationship). Provided that the initial ratio $^{226}Ra(0)/^{234}U$ at system closure remained invariant, all samples should plot, within error, on the $^{226}Ra(0)/^{234}U$ decay + ingrowth curve. This is, however, not the case, indicating that the initial $^{226}Ra(0)/^{234}U$ ratio varies from sample to sample (at least due to varying U-concentrations, Table 2) and cannot be used directly as a dating tool.

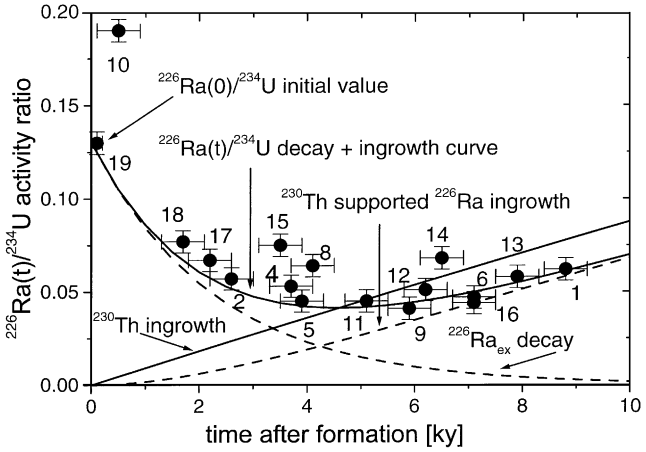

Fig. 6. Magnification of Fig. 3 showing the coupled ^{234}U/^{230}Th/^{226}Ra decay and ingrowth relationships for a short-term view from present day to 10 kyr ago. The activity ratios (^{226}Ra$_{ex}$/^{234}U)$_{sup}$ of the samples are also plotted as a function of their ^{230}Th/^{234}U ages (uncertainties: 2σ). It is obvious that the analytical data do not fit well to the ^{226}Ra(t)/^{234}U decay + ingrowth curve which indicates that the initial ^{226}Ra(0)/^{234}U is not uniform for all samples.

5.2.4. Comparison of the $^{226}Ra_{ex}/^{226}Ra(0)$ ages with the $^{230}Th/^{234}U$ ages

Since decay of the excess ^{226}Ra component follows first order exponential decay, i.e. ^{226}Ra$_{ex}(t) = {}^{226}$Ra(0)e$^{-\lambda 226t}$ the relationship presented in Eq. (10) can be rearranged in a similar manner to other dating systems based on decay of an excess component (such as ^{14}C/^{12}C dating), i.e. as ^{226}Ra$_{ex}$/^{226}Ra(0) or as follows:

$$\frac{^{226}\mathrm{Ra}_{ex}(t)}{^{226}\mathrm{Ra}(0)} = \frac{^{226}\mathrm{Ra}_{aut} - {}^{226}\mathrm{Ra}_{sup}(t)}{^{226}\mathrm{Ra}(0)} = \mathrm{e}^{-\lambda_{226}t} \qquad (12)$$

or resolved to the time of formation, respectively,

$$t_{age} = -\frac{1}{\lambda_{226}} \ln\left(\frac{^{226}\mathrm{Ra}_{aut} - {}^{226}\mathrm{Ra}_{sup}(t)}{^{226}\mathrm{Ra}(0)}\right). \qquad (13)$$

As shown in Eq. (6) the component ^{226}Ra$_{sup}(t)$ is dependent on time as well as on the specific ^{234}U activity of each sample. For the samples investigated here ^{226}Ra$_{sup}(t)$ was simply obtained using the sample ages determined individually via ^{230}Th/^{234}U. The resulting data are illustrated in Fig. 7 as ^{226}Ra$_{ex}(t)$/^{226}Ra(0) versus time, taking ^{226}Ra(0) = ^{226}Ra$_{aut}$ from the most recently formed travertine (#19) as the initial. All those samples which started with identical initials to #19 should plot on the theoretical ^{226}Ra$_{ex}$/^{226}Ra (0) decay curve. Indeed, most of the data plot on or close to the curve, and even samples which exhibit ages 4 times the half-life of ^{226}Ra still fit well to the decay curve. Note, that after correction for ^{226}Ra$_{sup}$ the residing component ^{226}Ra$_{ex}$ of the oldest samples (i.e. #1, 6, 13, 16) is extremely small (<0.1 mBq/g or $<3\times10^{-15}$ g/g), but still calculable within 30–50% uncertainty. From the youngest to the oldest samples the data cover a range of more than one order of magnitude with respect to ^{226}Ra$_{ex}(t)$/^{226}Ra(0).

Fig. 7 also includes the slope of the theoretical decay curve, $\lambda_{226} = 0.432\times10^{-3}/y$ (or $T_{1/2} = 1600$ yr, Firestone and Shirley, 1996) besides the regression fit through the data, which yields similar values for $\lambda_{226} = 0.444\times10^{-3}/y$ (or $T_{1/2} = 1560$ yr), indicating the consistency of the data to the decay curve ^{226}Ra$_{ex}(t)$/^{226}Ra(0). The intersection of the regression line with the y-axis yields $0.96 + 0.04$ which means that the ^{226}Ra(0) initial obtained from the most recently formed sample (#19, $t<0.1$ kyr), is supported by the mean through 16 further data points, strongly speaking for a similar initial ^{226}Ra(0) activity concentration in all samples.

The comparison of the ^{226}Ra$_{ex}$-ages to the ^{230}Th/^{234}U-ages is given in Fig. 8. It is indicated that the ^{230}Th/^{234}U chronometer becomes highly non-precise for samples <2 kyr ($2\sigma > 50\%$ for carbonates with only 3 vol% detritus inclusions, see Appendix A). On the other hand, precise results are obtained using ^{230}Th/^{234}U with increasing sample ages, while this time decay of ^{226}Ra$_{ex}$ reduces the precision of ^{226}Ra$_{ex}$/^{226}Ra(0). For those samples which have formed between 2 and 6 kyr ago (#2, 4, 5, 8, 15) both chronometers yield very similar ages and analytical uncertainties, which strongly suggests that ^{226}Ra$_{ex}$-dating of young Holocene samples is likely to be a good complementary method to ^{230}Th(t)/^{234}U.

5.2.5. Comparison of $^{226}Ra(0)$ with bulk chemical analyses

Although the isotope data argue for a uniform initial input of ^{226}Ra into the precipitating material, there is

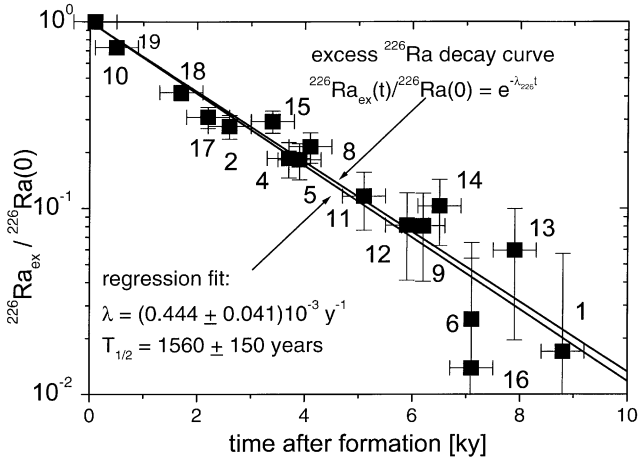

Fig. 7. Illustration of ^{226}Ra$_{ex}$/^{226}Ra(0) in semi-log scale as a function of time (uncertainties: 2σ). The regression analysis through the data results in a slope which is very similar to the theoretical ^{226}Ra decay curve and yields a half-life of 1560 + 150 yr, i.e. a value which is close to generally accepted value of 1600 yr (Firestone and Shirley, 1996).

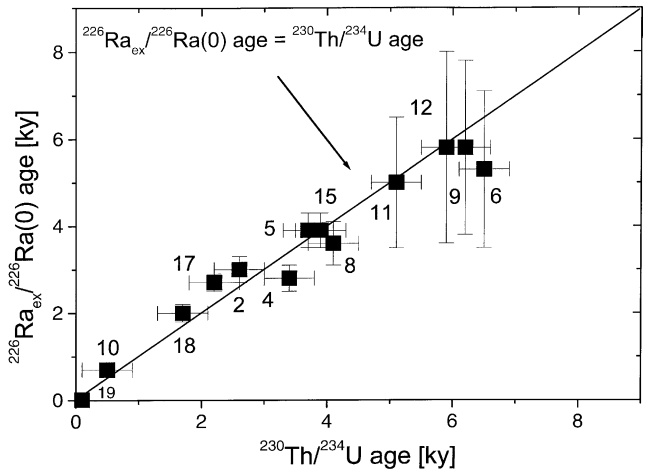

Fig. 8. Plot of the calculated $^{226}Ra_{ex}/^{226}Ra(0)$ formation ages versus the $^{230}Th/^{234}U$ ages (uncertainties: 2σ). The figure demonstrates the good agreement of the sample ages of travertine that has been formed 2–6 kyr before present.

further proof provided from the bulk chemical analysis to justify this conclusion. Table 4 summarizes the major ionic components in 6 travertine samples and in the groundwater. The minor constituents are not shown, because their contributions were found to be very low and almost below the analytical detection limits (traces of Fe, Si, Mn, Al, P, Cu, Cr, etc. <0.005 mg/g). Only sample 10 contains significant traces of Si and Al of ca. 0.01 mg/g, indicating impurities of the calcite with silicate material (probably of clay mineralogical composition). These additions are consistent with the higher concentration of ^{232}Th in #10 (Table 2) compared to the other five pure calcite samples presented in Table 4 (#2, 4, 12, 13, 19). Assuming similar densities of detritus and pure travertine, as well as comparable concentrations of uranium in both phases, the detrital contribution in sample #10 amounts to about 5–10%, while in all other samples this contribution is less than 1%. The concentrations of Ca^{2+} confirm this conclusion because the $Ca/CaCO_3$ weight ratio of pure calcite is 0.40 and this value was obtained for the five pure travertine samples. The authigenic phase is hence pure calcite in which about 1% of the cations (i.e. Ca^{2+}) is substituted by Mg^{2+}. There is, in addition, a slight contribution of SO_4^{2-} to the anions (CO_3^{2-}). The latter forms probably individual phases, such as celestite ($SrSO_4$), which is a typical low temperature mineral associated in limestone formations (Hurlbut and Klein, 1977). Presence of such phases could explain the higher variability of Sr^{2+} in comparison to all the other earth alkaline elements (Mg^{2+}, Ba^{2+}).

In particular, as Ra is an earth alkaline element behaving chemically similar to Ba, it is interesting to study the variation of Ba in the rock samples. Since the concentration of Ca in the authigenic carbonate phase is uniform it is most suitable to use the Ba/Ca ratios as a measure of the variability of Ba in the authigenic material. As Fig. 5 indicates, this ratio is highly constant $(0.49+0.02)\times10^{-3}$ for all six samples and no trend with sample age can be observed, which corroborates the conclusion made above of uniform initial $^{226}Ra(0)$ with time. It is also interesting to note that the Ra/Ba ratio in the water is very similar to that in the most recently formed samples, #19, i.e. $(Ra/Ba)_{water}/(Ra/Ba)_{19}=1.4$. This indicates that the co-precipitation yield is similar for these homologue elements.

5.2.6. Calculation of $^{226}Ra_{ex}$ ages for samples with unknown $^{226}Ra_{sup}$

As shown in the right term of Eq. (13) calculation of $^{226}Ra_{ex}/^{226}Ra(0)$ ages depend on the component $^{226}Ra_{sup}(t)$, which changes with time. To obtain an estimate on the fraction of the component $^{226}Ra_{sup}$ (supported from ^{234}U and ^{230}Th) on total ^{226}Ra in the authigenic phase, we plotted the ratio ($^{226}Ra_{sup}/^{226}Ra_{ex}+^{226}Ra_{sup}$) as a function of the time since system closure and for different initial $^{226}Ra(0)/^{234}U$ activity ratios of 0.2, 0.5 and 1.0 (Fig. 9). It is obvious that for sample ages ranging from present to 2000 yr before present, the fraction of $^{226}Ra_{sup}$ on total ^{226}Ra is fairly low ($<10\%$) but, for formation ages preceding that time, a correction for $^{226}Ra_{sup}$ becomes essential, especially if the samples started with low initial $^{226}Ra(0)/^{234}U$ ratios. To circumvent rather extensive iteration procedures, we present a more practical way to calculate $^{226}Ra_{ex}$-ages via expression of Eq. (12) as difference of two terms, i.e.,

$$F(t)=\frac{^{226}Ra_{aut}-{}^{226}Ra_{sup}(t)}{^{226}Ra(0)}-e^{-\lambda_{226}t}. \quad (14)$$

Our consideration is as follows: If $F(t)=0$, it is required that both terms in Eq. (12) have to give identical values. Such a situation exists at one fixed moment, which is exactly the time of the mineral formation. The function $F(t)$ can be calculated with time as the free parameter, if $^{226}Ra_{aut}$, $^{226}Ra(0)$ as well as U and Th isotopes have been determined analytically. The age is obtained from the intersection of $F(t)$ with the horizontal line where $F(t)=0$. To demonstrate this we present, in Fig. 10, an illustration on the evolution of $F(t)$. Two examples are shown, (i) a $^{226}Ra_{aut}/^{226}Ra$ (0) activity ratio of 0.5 (termed type A curve series) and (ii) $^{226}Ra_{aut}/^{226}Ra(0)=0.25$ (type B curve series). Series A and B split into four separate curves marked with the indices 0 to 3 which refer to different initial $^{226}Ra(0)/^{234}U$ ratios of 0.2, 0.5, 1.0 and ∞, respectively. For both curve type series it is shown that with increasing concentration of uranium, the component $^{226}Ra_{sup}$ contributes more to $^{226}Ra_{aut}$ which increases the $^{226}Ra_{ex}/^{226}Ra(0)$ age.

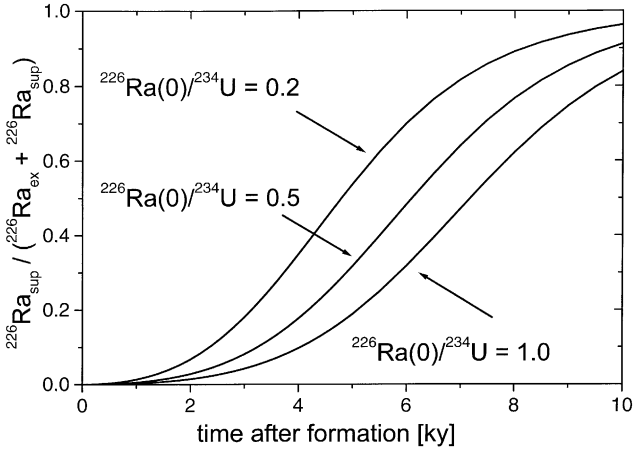

Fig. 9. Fraction of the precursor supported ^{226}Ra over total Ra (supported + excess) with time. Extremely low contributions of the $^{226}Ra_{sup}$ component are indicated for systems which are younger than two half-lives of ^{226}Ra or which started with similar activities of ^{226}Ra and ^{234}U.

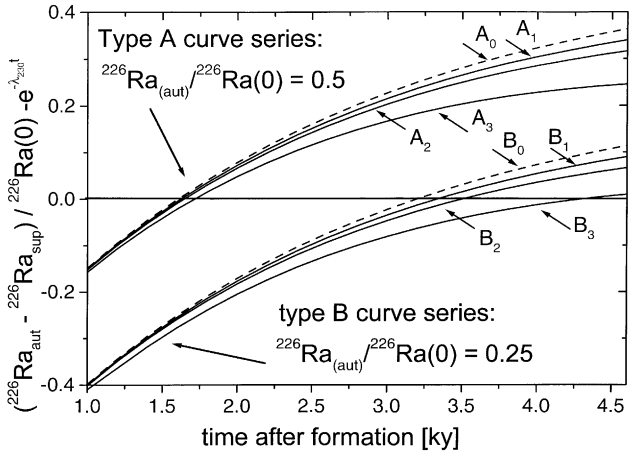

Fig. 10. Model examples showing the difference between the time dependent quantities ($^{226}Ra_{ex} = ^{226}Ra_{aut} - ^{226}Ra_{sup}(t)$) and $^{226}Ra(0)e^{-\lambda 226t}$ as a function of the time since sample formation. The correct age is obtained when both terms are equal, or the difference is zero. Type A curves hold for samples with $^{226}Ra_{aut}/^{226}Ra(0) = 0.5$, type B curves for samples with $^{226}Ra_{aut}/^{226}Ra(0) = 0.25$. The indices 0, 1, 2, 3 refer to $(^{226}Ra/^{234}U)_{aut}$ ratios of 0.2, 0.5, 1.0 and ∞, respectively.

5.2.7. *Excesses of ^{210}Po on sample surfaces and check on closed system behavior*

As noted in the analytical section, recent infiltration of rainwater may lead to a significant disequilibrium between ^{226}Ra and ^{210}Pb-^{210}Po on the rock surfaces. One fine grained sample with a highly porous surface (#7), which could not be purified mechanically confirms this observation. Analysis of ^{226}Ra via emanation of short-lived ^{222}Rn ($T_{1/2} = 3.8$ d) into a liquid scintillation cocktail yielded a value which is much closer to the expected ^{226}Ra activities of material with comparable formation ages (#4, 5, 8, 11, 12) while ^{210}Po - ^{210}Pb is in large excess. Since it cannot be ruled out that the surface of #7 exhibits additional slight excesses of sorbed ^{226}Ra, this sample was not included in the comparison between U/Th-ingrowth and Ra_{ex}-decay ages. On the other hand, for samples with abraded surfaces (i.e. for which surface effects causing isotope disequilibrium could be ruled out) combined analysis of ^{210}Po and ^{222}Rn is helpful for the selection of very young samples < 100 yr, if ^{210}Po (as a measure for ^{210}Pb) and ^{222}Rn (for ^{226}Ra) are not in secular equilibrium. Such samples are useful to obtain a value for ^{226}Ra(0) and a good example for short-term disequilibrium between ^{210}Pb and ^{226}Ra is indicated for sample #19 (fresh precipitated limestone covering a 10 yr old electric wire).

The use of taking ^{210}Po (advantage: "fast chemistry") besides ^{222}Rn as a measure of ^{226}Ra in samples with formation ages exceeding 5 times the half-life of ^{210}Pb or $t > 100$ yr is a tool to demonstrate closed system behavior, if both isotopes yield identical activity concentrations. We therefore additionally selected 5 abraded samples (#2, 4, 5, 10, 14/1) for analysis via the ^{222}Rn emanation method. The data in Table 3 clearly show that the activity ratio of ^{210}Po/^{222}Rn (or ^{210}Pb/^{226}Ra) is almost unity or that these nuclides are in secular equilibrium. Closed system behavior can also be investigated if much older sample material is considered, because in samples as old as 7 kyr 97% of authigenic ^{226}Ra is supplied from ^{230}Th, i.e $^{226}Ra_{aut} \approx ^{226}Ra_{sup}$. If there would be leakage of the rare gas ^{222}Rn through the crystal lattice one would measure a much lower apparent ^{226}Ra content (or calculate negative ages). However, as the data show, there is no visible trend indicating preferential loss of ^{222}Rn.

6. Geological evolution of the travertine deposit

The results of ^{230}Th/^{234}U as well as $^{226}Ra_{ex}/^{226}Ra(0)$ dating of tufaceous freshwater limestone and travertine coatings inside caves contribute in understanding the origin of the Hell Grottoes cave system. The isotope data confirm the assumption that the Hell Grottoes travertine formed in the last 9000 yr in common with other freshwater limestone complexes in Europe (e.g. Krka Falls, Yugoslavia). The highest limestone deposition rate was probably during the Holocene climate optimum (Hypsithermal) between 8000 and 5500 yr when about 80–90% of the limestone complex was built up. Subsequently, the tufaceous limestone precipitation decreased dramatically, and in the last few thousand years there has been only little limestone precipitation on the surface, while in the closed cavities travertine flow-layers were formed and stalagmite nodules started to grow. Our interpretation of the growth history of the

travertine deposit is based on the geographic location from where the samples were taken as well as their ages. In addition, considering the stratigraphic sequence of the limestone complex, we added isolines of identical age to the geological profile shown in Fig. 1. Clearly, such isolines remain somewhat speculative because the structure of the limestone complex is similar and because large parts were removed previously (and no samples were preserved during the mining activity).

Our interpretation of a strong decrease of the tufaceous limestone precipitation in the last few thousand years is most presumably caused by a change of the vegetation in the water recharge area in the Lorze Valley which is a large moor. During the Holocene this moor gradually grew from a fen to a bog which still exists today. The appearance of the limestone precipitation is directly connected with the development of the moor. In the fen, the percolating rainwater is acidified by uptake of CO_2 from decomposition of organic matter and by formation of humic acids. As soon as such acidified waters come into contact with the underlying clastic limestone sediments, some lime will dissolve and dissociate. Consequently, when the groundwater discharges again, carbon dioxide escapes into the atmosphere and, due to a rise in pH, limestone starts to precipitate. However, with the change of a fen to a much thicker bog, less water can percolate through the underlying sediments, because with thickness the moor becomes less transmissive which causes storage of the water and surface run-off. This situation is shown schematically in Fig. 11 where the relative precipitation rate of limestone according to our view is given along with literature based relative precipitation rate of rainwater and change in temperature over the last 10,000 yr (Patzelt, 1995; Burga and Perret, 1998). The tremendous decrease of the limestone formation in more recent times is most likely due to a rapid change of the shallow moor to a massive bog in the cause of pronounced rainfall in the early Atlantikum. If this explanation is valid throughout, the isotope ages also fix the change in the moor from a fen to a bog at the end of the Holocene climate optimum.

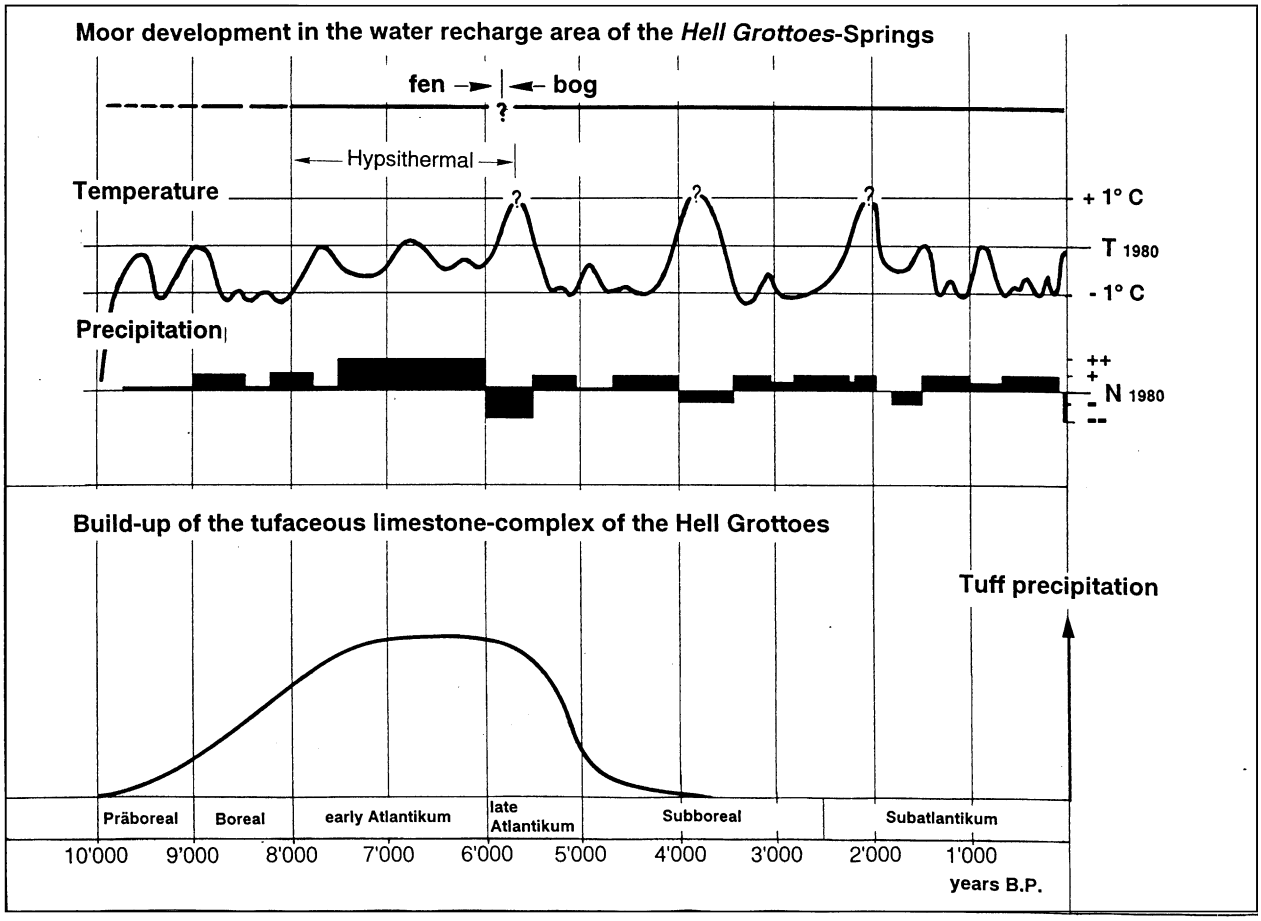

Fig. 11. Schematic reconstruction of the growth evolution of the limestone complex of the Hell Grottoes and the development of the catchment area from a fen to a bog in the cause of temperature increase and high rainfall intensities during the early Atlantikum. The temperature curves and relative water precipitation data are redrawn after Patzelt (1995).

7. Conclusions

^{238}U series disequilibrium dating of young tufaceous freshwater travertine from the limestone caves Hell Grottoes at Lucerne, Switzerland yielded ^{230}Th/^{234}U formation ages ranging from recent time to about 9 kyr ago and therefore indicate that the authigenic deposit was formed during global warming in the Holocene. The major part of the limestone complex formed during a warm and humid period 8000–6000 yr before present and the travertine filling of the caves extended to about 3000 yr b.p. Correction of slight impurities of detrital silicates in the authigenic travertine via U/Th isochron relationships yielded almost identical ^{232}Th/^{234}U ratios for the silicate material, thus allowing the same correction procedure to be applied for all samples (i.e. internal isochrons to obtain one age for several co-genetic samples were unnecessary). The resulting individual ages of about 20 calcite samples hence sufficed to reconstruct the geological history of this deposit.

The ages obtained by ^{230}Th/^{234}U ingrowth-dating were then used to test the applicability of the ^{226}Ra$_{ex}$/^{226}Ra(0) chronometer that is based on decay of excess ^{226}Ra in the authigenic precipitates. This chronometer is most suitable to investigate samples that formed between a few hundred years and up to about 7000 yr ago, corresponding to 4–5 half-lives of ^{226}Ra and therefore fits ideally into the time gap between the two established U-series chronometers, i.e. ^{210}Pb (suitable from 0–100 yr) and ^{230}Th/^{234}U (from 4–200 kyr, see Appendix A). For further investigations it is recommended to use the same sample material which is suitable for ^{230}Th/^{234}U chronology studies (e.g. speleothem such as calcite tuffs, marine phosphorites or biochemical formed materials as corals, etc.). If the U and Th isotope analyses show that the sample material does not contain significant quantities of inherited ^{230}Th(0), ^{226}Ra$_{ex}$/^{226}Ra(0) dating can strongly support ^{230}Th/^{234}U, in particular if young samples are strongly intergrown with detrital impurities. However, to obtain geologically meaningful ^{226}Ra$_{ex}$/^{226}Ra(0) ages, the initial value of incorporated excess ^{226}Ra, i.e. ^{226}Ra(0), has to be uniform independent of the time of system closure. To study the stability of uniform ^{226}Ra(0) over time it is further useful to determine the concentration of the chemically analogous behaving element Ba as well (normalization isotope) and, if ^{210}Po is taken as a measure for ^{226}Ra, sample surfaces should be abraded to exclude excesses of sorbing ^{210}Po or ^{210}Pb, introduced by surrounding present day groundwater, on surface sites.

Acknowledgements

We wish to thank H. Schmid for the permission to take samples from the historical limestone cave. We also acknowledge with thanks the discussions with Ch. Schuler, G. Butterweck and N.E.A. Crompton during preparation of this work, the support by R. Kündig for figure painting and the critical review performed by J. Kramers, P. Rowe and C. Schluechter. This research was partially supported by the Swiss Inspectorate for the Safety of Nuclear Installations, HSK.

Appendix A. Evaluation of the analytical uncertainties in ^{234}U–^{230}Th–^{226}Ra dating

A.1. The system ^{230}Th/^{234}U

The evaluation of the overall analytical uncertainties in radiochemistry include statistical or random errors from counting radioactive decay as well as systematic errors resulting from laboratory operations and from uncertainties of the activity concentrations of radionuclide calibration tracers (spikes) which are used for isotope dilution analysis (Taylor, 1982; Faure, 1986; Ivanovich and Murray, 1992; Attendorn and Bowen, 1997). The random uncertainties (or type A, see Seymour et al., 1992; ISO, 1995) can be calculated by considering the total counted net impulses I_i of any nuclide with mass number i (here $i = {}^{230}$Th, ^{232}Th, ^{234}U, ^{238}U, ^{210}Po) and J_i of the isotope dilution spikes (^{228}Th, ^{232}U, ^{209}Po). For ultra low level counting systems the absolute uncertainty σ of a measured α-peak is given by the Poisson distribution, i.e. $\sigma = \sqrt{I_i}$ which is justified since background pulses (I_0) using high-purity α-detectors are insignificant compared to the measured count rates of the sample nuclides (typically in this work for the peak region of ^{234}U: $I_0 < 5$, $I_{234} \approx 5000$ counts under the counting conditions as given below). Following the law of error propagation for the division of two measured quantities (for instance for a spiked uranium analysis) the uncertainty on the sample/spike ratio, I_{234}/J_{232} is given as follows:

$$\sigma\left(\frac{I_{234}}{J_{232}}\right) = \frac{I_{234}}{J_{232}}\sqrt{\frac{(\Delta I_{234})^2}{I_{234}^2} + \frac{(\Delta J_{232})^2}{J_{232}^2}} \tag{A.1}$$

or, with $\sigma = \sqrt{I_i}$, a more simplified expression is obtained (cf. Wilson, 1965)

$$\sigma\left(\frac{I_{234}}{J_{232}}\right) = \frac{I_{234}}{J_{232}}\sqrt{\frac{1}{I_{234}} + \frac{1}{J_{232}}}. \tag{A.2}$$

For calculation of a sample nuclide activity such as ^{234}U using reference ^{232}U-spike additions, the following relation holds (A.3):

$$a_{234} = \frac{I_{234}}{J_{232}} a_{232}. \tag{A.3}$$

The same relation holds for calculation of the Th isotopic composition (^{232}Th, ^{230}Th) in the sample adding

^{228}Th-yield tracer. Therefore, if two uncoupled radiospikes of U and Th are used, the overall statistical uncertainty error on U-, Th-nuclides or U/Th isotope ratios has to consider the (statistical) uncertainty of the true value of the spike activity, Δa_i which has to be added as $(\Delta a_i/a_i)^2$ into Eq. (A.2). However, in α-spectrometry this problem can be circumvented, if a coupled long-lived mother–short-lived daughter spike pair, at or close to secular equilibrium, is taken for isotopic dilution analysis (such as ^{232}U/^{228}Th with half-lives of $T_{1/2} = 68$ and 1.8 yr). Providing secular equilibrium condition the ^{230}Th/^{234}U activity ratio can be calculated precisely even without exact knowledge of the spike nuclide activities and with $a_{232} = a_{228}$ the following relation results for the ^{228}Th/^{234}U activity ratio

$$\frac{a_{230}}{a_{234}} = \frac{I_{230}}{I_{234}}\frac{J_{232}}{J_{228}}. \tag{A.4}$$

Partial derivation according to the law of error propagation yields

$$\sigma\left(\frac{a_{230}}{a_{234}}\right) = \frac{I_{230}}{I_{234}}\frac{J_{232}}{J_{228}}\sqrt{\frac{1}{I_{230}} + \frac{1}{I_{234}} + \frac{1}{J_{228}} + \frac{1}{J_{232}}}. \tag{A.5}$$

For calculation of the uncertainty of ^{230}Th/^{234}U formation ages, the mother/daughter growth relation $^{230}\mathrm{Th}(t) = {}^{234}\mathrm{U}(1 - \mathrm{e}^{-\lambda_{230}t})$ has to be solved for t. Rearranging this expression and considering the measured counts I_i and J_i instead of activities it follows:

$$t = -\frac{1}{\lambda_{230}}\ln\left(1 - \frac{I_{230}}{I_{234}}\frac{J_{232}}{J_{228}}\right). \tag{A.6}$$

Considering all internal and external derivations the following expression is finally obtained:

$$\sigma(t) = \frac{1}{\lambda_{230}}\frac{1}{\dfrac{I_{234}}{I_{230}}\dfrac{J_{228}}{J_{232}} - 1}\sqrt{\frac{1}{I_{230}} + \frac{1}{I_{234}} + \frac{1}{J_{228}} + \frac{1}{J_{232}}}. \tag{A.7}$$

Relation (A.7) is valid only for ideal systems containing pure, authigenic minerals. However, such ideal conditions do not relate to the travertine analyzed here because the authigenic young carbonate phase were always found to be mixed with some (old) detrital material containing ^{232}Th and ^{238}U in secular equilibrium with all their progeny nuclides. Since in this case the activity of ^{234}U is equal to that of the daughter ^{230}Th (i.e. $a_{234} = a_{230}$), correction of detrital impurities from measured ^{230}Th is simply obtained as follows:

$$I_{230,\mathrm{cor}} = I_{230,\mathrm{m}} - kI_{232}, \tag{A.8}$$

where the subscripts cor and m refer to the detritus corrected and measured impulses of ^{230}Th and k to the (^{230}Th/^{232}Th) ratio in the detritus component. Incorporating the correction term for detritus contribution into Eq. (A.6), the partial differentiation yields

$$\sigma(t) = \frac{1}{\lambda_{230}}\frac{1}{\dfrac{I_{234}}{I_{230,\mathrm{cor}}}\dfrac{J_{228}}{J_{232}} - 1} \times \sqrt{\frac{I_{230,\mathrm{m}} + k^2 I_{232}}{I_{230,\mathrm{cor}}^2} + \frac{1}{I_{234}} + \frac{1}{J_{228}} + \frac{1}{J_{232}}}. \tag{A.9}$$

To calculate the uncertainty of ^{230}Th/^{234}U dating for typical sample material analyzed here (Fig. 12), we inserted the following typical values for the parameters in Eq. (A.9): ^{234}U = 6 mBq/g, sample weight = 4 g, counting efficiency = 35%, chemical recovery = 95%, total counting time = one week. This yields $I_{234} \approx 5000$ counts. I_{230} was calculated using $I_{230}(t) = I_{234}(1 - \mathrm{e}^{-\lambda_{230}t})$. Furthermore, since the chemical recoveries were comparable for U and Th we inserted $J_{228}/J_{232} = 1$; and to demonstrate the effect of detrital contribution to authigenic material, we plotted a sequence of sample mixtures with different ^{234}U/^{232}Th ratios ranging from 500 to 10, or (with $k = 1.3 + 0.1$) relative contributions of authigenic uranium of as high as 99 to 87% on the total sample mixture (Fig. 12). From this plot it is obvious that samples with ^{234}U/^{232}Th ratios of 10 and below are not suitable for U/Th dating if the sample age is below 5 kyr. For travertine that precipitated about 30 kyr ago, the relative uncertainty is passing through a minimum and for formation ages above that value, the ^{230}Th/^{234}U ratio rapidly progresses towards secular equilibrium (leading to $I_{234}/I_{230} \to 1$, i.e. $\sigma(t) \to \infty$), while in the right term in Eq. (A.9) the component $I_{230,\mathrm{cor}}$ becomes similar to $I_{230,\mathrm{m}}$ with progressing t, because then significant quantities of ^{230}Th have been built in that exceed by far detrital ^{230}Th.

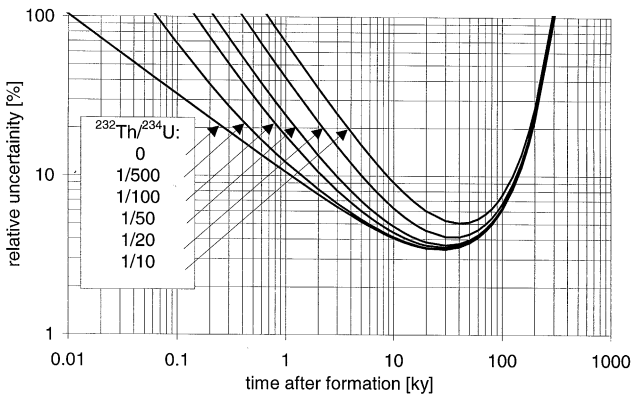

Fig. 12. Illustration of the relative uncertainty (2σ) of ^{230}Th/^{234}U ages with time for different measured ^{232}Th/^{234}U ratios off $\frac{1}{10} - \frac{1}{500}$. This chronometer is limited for ages below 3–4 kyr, especially with increasing contribution of detrital impurities (given as ^{232}Th/^{234}U ratio), while with increasing sample age the influence of detritus additions are less significant. For ages above 100 kyr the uncertainty increases again because the ^{230}Th activity tends towards secular equilibrium with ^{234}U.

A.2. The system $^{226}Ra_{ex}/^{226}Ra(0)$

In contrast to $^{230}Th/^{234}U$ this chronometer requires at least two samples for determining (i) $^{226}Ra_{ex}$ in the material to be dated and (ii) $^{226}Ra(0)$ in very young samples in which decay of $^{226}Ra(0)$ is of importance. As described above, radioassay of both samples is performed using yield spike isotopes (i.e. ^{209}Po besides ^{210}Po). Providing secular equilibrium between ^{210}Po and ^{226}Ra, 4 measured quantities have to be considered, that are, $I_{210(s)}$ = total counts of ^{210}Po in the sample to be dated, $J_{209(s)}$ = total counts of the ^{209}Po isotope dilution spike in the sample, $I_{210(i)}$ = total counts of ^{210}Po in the sample taken as initial and, $J_{209(i)}$ = total counts of the ^{209}Po isotope dilution spike in the sample taken as initial. To calculate the $^{226}Ra_{ex}/^{226}Ra(0)$ activity ratios, analogous equations to (A.1)–(A.4) can be applied yielding

$$\frac{a_{226,ex}}{a_{226,0}} = \frac{I_{210(s)}}{J_{209(s)}}\frac{J_{209(i)}}{I_{210(i)}}R_{209}, \tag{A.10}$$

where R_{209} is the activity ratio of the spike in the sample to be dated and the initial sample. Since a sample age is obtained using $t = -1/\lambda_{226}\ln(^{226}Ra_{ex}/^{226}Ra(0))$, the statistical uncertainty on the time t has to be performed via derivation of all quantities listed in the right term of Eq. (A.10), which yields

$$\sigma(t) = \frac{1}{\lambda_{226}} \times \sqrt{\frac{1}{I_{210(s)}} + \frac{1}{I_{210(i)}} + \frac{1}{J_{209(s)}} + \frac{1}{J_{209(i)}} + \frac{\Delta R_{209}^2}{R_{209}^2}}. \tag{A.11}$$

Considering additional correction for detrital contamination (c.f. Eq. (A.8)) it follows for the uncertainty of an $^{226}Ra_{ex}/^{226}Ra(0)$ age

$$\sigma(t) = \frac{1}{\lambda_{226}}\sqrt{\frac{I_{210(s),m} + k^2 I_{232(s)}}{I_{210(s),cor}^2} + \frac{1}{I_{201(i),m}} + \frac{\Delta I_{210(s),sup}^2}{I_{210(s),cor}^2} + \frac{I_{232(s)}^2}{I_{210(s),cor}^2}\Delta k^2 + \frac{\Delta R_{209}^2}{R_{209}^2}}. \tag{A.12}$$

In contrast to $^{230}Th/^{234}U$ it is obvious that the detritus correction increases the uncertainty in $^{226}Ra_{ex}$-dating less significantly, however, the initial $^{226}Ra(0)/^{234}U$ ratio has a strong influence on the accuracy of the sample ages using this chronometer (Fig. 13).

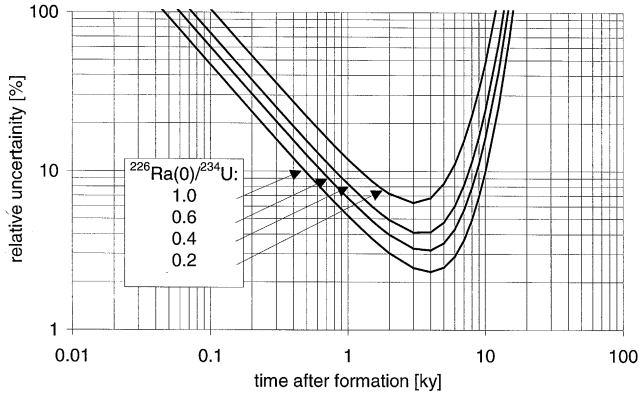

Fig. 13. Illustration of the relative uncertainty (2σ) of $^{226}Ra_{ex}/^{226}Ra$ ages with time for different initial $^{226}Ra(0)/^{234}U$ values of 0.2–1.0. It is shown that this chronometer is most suitable for samples which have been formed between about 0.5 and 6 kyr ago. In the optimum time range (i.e. between 1 and 6 kyr) the total analytical uncertainty can be as low as a few percent.

References

Allègre, C.J., Condomines, M., 1976. Fine chronology of volcanic processes using ^{238}U–^{230}Th systematics. Earth and Planetary Science Letters 28, 5395–5406.

Anderson, P., Wasserburg, G.J., Chen, J.H., Papanstassiou, D.A., Ingri, J., 1995. ^{238}U–^{234}U and ^{232}Th–^{230}Th in the Baltic Sea and in river water. Earth and Planetary Science Letters 130, 217–234.

Attendorn, H.G., Bowen, R.N.C., 1997. Radioactive and Stable Isotope Geology. Chapman & Hall, London, 522pp.

Bajo, S., Eikenberg, J., 1999. Elektrodeposition of actinides for α-spectrometry. Journal of Radioanalytical and Nuclear Chemistry 242, 745–751.

Bischoff, J.L., Julia, A.R., Mora, A., 1988. Uranium-series dating of the Mousterian occupation at Abric Romani, Spain. Nature 332, 68–70.

Bischoff, J.L., Fitzpatrick, J.A., 1991. U-series dating of impure carbonates: an isochron technique using total-sample dissolution. Geochimica Cosmochimica Acta 55, 543–554.

Burga, C.A., Perret, R., 1998. Vegetation und Klima der Schweiz seit dem juengerem Eiszeitalter. Ott, Thun, Switzerland, 805pp. (in German).

Burnett, W.C., Baker, K.B., Chin, P.A., McCabe, W., Ditchburn, R., 1988. Uranium Series and AMS ^{14}C studies of modern phosphatic pellets from Peru shelf muds. Marine Geology 80, 215–230.

Chabaux, F., Allègre, C.J., 1994. ^{238}U–^{230}Th-^{226}Ra disequilibria in volcanics: a new insight into melting conditions. Earth and Planetary Science Letters 126, 61–74.

Condomines, M., Hémond, C., Allègre, C.J., 1988. U–Th–Ra radioactive disequilibria and magmatic processes. Earth and Planetary Science Letters 90, 242–262.

Edwards, R.L., Chen, J.H., Wasserburg, G.J., 1987. ^{238}U–^{234}U–^{230}Th–^{232}Th systematics and the precise measurement of time over the past years. Earth and Planetary Science Letters 81, 175–192.

Eikenberg, J., Bajo, S., Zumsteg, I., Ruethi, M., Fern, M.J., 1999. Fast radiochemical screening of transuranium nuclides in urine using actinide extractive resin and low level α/β-LSC. Radioactivity and Radiochemistry 10 (3), 19–31.

Eikenberg, J, Tricca, A., Vezzu, G., Stille, P., Bajo, S., Ruethi, M., 2001a. $^{228}Ra/^{226}Ra/^{224}Ra$ and $^{87}Sr/^{86}Sr$ relationships for determining interactions between ground and river water in the Upper Rhine Valley. Journal of Environmental Radioactivity, 54, 133–162.

Eikenberg, J, Tricca, A., Vezzu, G., Bajo, S., Ruethi, M., Surbeck, H., 2001b. Determination of ^{228}Ra, ^{226}Ra and ^{224}Ra in natural water via adsorption on MnO_2-coated discs. Journal of Environmental Radioactivity, 54, 109–131.

Faure, G., 1986. Principles of Isotope Geology. Wiley, New York.

Firestone, R.B., Shirley, V.S., 1996. . Table of Isotopes, Vol. 2. Wiley, New York.

Fuger, J., Oetting, F.L., 1976. The chemical thermodynamics of actinide elements and compounds, part 2, the actinide aqueous ions. International Atomic Energy Agency, IAEA-publication, STI/PUB/424/2.

Gill, J.B., Pyle, D.M., Williams, R.W., 1992. Igneous rocks. In: Ivanovich, M., Harmon, S. (Eds.), Uranium Series Disequilibrium. Oxford Science Publisher, Clarendon Press, Oxford, pp. 207–258.

Harada, K., Burnett, W.C., LaRock, P.A., Cowart, J.B., 1989. Polonium in Florida groundwater and its possible relationship to the sulfur cycle and bacteria. Geochimica Cosmochimica Acta 53, 143–150.

Heim, A., 1919. Geologie der Schweiz I. Technitz Berlin, Leipzig.

Horwitz, E.P., Dietz, M.L., Chiarizia, R., Diamond, H., 1993. Separation and preconcentration of actinides from acidic media by extraction chromatography. Analytica Chimica Acta 281, 361–372.

Hurlbut, C.S., Klein, C., 1977. Manual of Mineralogy. Wiley, New York, 532pp.

ISO, 1995. Guide to the Expression of Uncertainty in Measurement, 1st Edition. International Organisation for Standardization, 1995, 101pp., ISBN 92–67–10188–9.

Israelson, C., Björck, S., Hawkesworth, C.J., Possnert, G., 1997. Direct U–Th dating of organic- and carbonate-rich sediments from southern Scandinavia. Earth and Planetary Science Letters 153, 251–263.

Ivanovich, M., Murray, A., 1992. Spectrometric methods. In: Ivanovich, M., Harmon, S. (Eds.), Uranium Series Disequilibrium. Oxford Science Publisher, Clarendon Press, Oxford, pp. 127–173.

Kaufman, A., Broecker, W.S., 1965. Comparison of ^{230}Th and ^{14}C ages for carbonate materials from Lakes Lahontan and Bonneville. Journal of Geophysical Research 70, 4039–4054.

Kaufman, A., 1993. An evaluation of several methods for determining $^{230}Th/U$ ages in impure carbonates. Geochimica Cosmochimica Acta 57, 2303–2317.

Kaufman, A., Wasserburg, G.J., Porcelli, D., Bar-Matthews, M., Ayalon, A., Halicz, L., 1998. U–Th isotope systematics from the Soreq cave, Israel and climatic correlation. Earth and Planetary Science Letters 156, 141–155.

Kim, K.H., Burnett, W.C., 1985. ^{226}Ra in phosphate nodules from the Peru/Chile seafloor. Geochimica Cosmochimica Acta 49, 1073–1081.

Koide, M., Bruland, K., Goldberg, E.D., 1976. ^{226}Ra chronology of a coastal marine sediment. Earth and Planetary Science Letters 31, 31–36.

Krauskopf, K.B., 1979. Introduction to Geochemistry. McGraw-Hill Kogakusha, 617pp.

Langmuir, D., 1978. Uranium solution-mineral equilibria at low temperatures with application to sedimentary ore deposits. Geochimica Cosmochimica Acta 42, 547–569.

Langmuir, D., Herman, .J.S., 1980. The mobility of Thorium in natural waters at low temperatures. Geochimica Cosmochimica Acta 44, 1753–1766.

Latham, A.G., Schwarcz, H.P., Ford, D.C., 1986. The paleomagnetism and U–Th dating of Mexican stalagmite, DAS2. Earth and Planetary Science Letters 79, 195–207.

Latham, A.G., Schwarcz, H.P., 1992. Carbonate and sulfate precipitates. In: Ivanovich, M., Harmon, S. (Eds.), Uranium Series Disequilibrium. Oxford Science Publisher, Clarendon Press, Oxford, pp. 423–459.

Luo, S., Ku, T.-L., 1991. U-series isochron dating: a generalized method employing total-sample dissolution. Geochimica Cosmochimica Acta 55, 555–564.

MacDougall, J.D., 1995. Using short-lived U and Th series isotopes to investigate volcanic processes. Annual Review of Earth and Planetary Sciences 23, 143–167.

Moore, W.S., Astwood, H., Lindstrom, C., 1995. Radium isotopes in costal waters of the Amazon shelf. Geochimica Cosmochimica Acta 59, 4285–4298.

OECD, 1992. In: Wanner, H., Forest, I. (Eds.), Chemical Thermodynamics of Uranium. North-Holland, Amsterdam, 715pp.

Oldfield, F., Appleby, P.G., Batterbee, R.W., 1978. Alternative ^{210}Pb dating: results from the New Guinea Highlands and Lough Erne. Nature 271, 339–342.

Osmond, J.K., Ivanovich, M., 1992. Uranium-series mobilisation and surface hydrology. In: Ivanovich, M., Harmon, S. (Eds.), Uranium Series Disequilibrium. Oxford Science Publisher, Clarendon Press, Oxford, pp. 259–289.

Patzelt, H., 1995. 1st Day: July 23rd; Stops1–5. In: Van Husen, D. (Ed.), Eastern Alps Travers INUQUA 1995, Quaternary field trips in Central Europe, Vol. 7, pp. 381–434.

Plater, A.J., Ivanovich, M., Dugdale, R.E., 1995. ^{226}Ra contents and $^{228}Ra/^{226}Ra$ activity ratios of the Fenland rivers and The Wash, eastern England: spatial and seasonal trends. Chemical Geology 119, 275–292.

Radfern, D., 1996. The MAPLE Handbook. Springer, New York, ISBN 0–387–94538–5.

Robbins, J.A., 1978. Geophysical and geochemical applications of radioactive lead. In: Niagru, J.O. (Ed.), The Biochemistry of Lead in the Environment, Vol. 1A. Elsevier, Amsterdam.

Romano, R., Taddeucci, A., Voltaggio, M., 1987. Uranium series dating of some travertines from the south-western flank of Mt. Etna. Rendiconi della Società Italiana di Mineralogia et Petrologia 42, 249–256.

Seymour, R., Sergent, F., Knight, K., Kyker, B., 1992. Impact of sensitivity and throughput on optimum selection of a low-background alpha/beta gross counting system. Radioactivity and Radiochemistry 3, 14–27.

Sturchio, N.C., Binz, C.M., 1988. Uranium-series age determination of calcite veins VC-1 drill core, Valles Caldera, New Mexico. Journal of Geophysical Research 93, 6097–6102.

Sturchio, N.C., 1990. Radium isotopes, alkaline earth diagenesis, and age determination of travertine from mammoth hot springs, Wyoming USA. Applied Geochemistry. 5, 631–640.

Taylor, J.R., 1982. An Introduction to Error Analysis. Oxford University Press, USA.

Tricca, A., 1997. Transport mechanisms of trace elements in surface and ground water: Sr, Nd, U and REE evidence. Ph.D. Thesis, University Louis Pasteur Strasbourg, France, 234pp.

Volpe, A.M., Hammond, P.E., 1991. $^{238}U–^{230}Th–^{226}Ra$ disequilibria in young Mount St. Helens rocks: time constraint for magma formation and crystallization. Earth and Planetary Science Letters 107, 475–486.

Volpe, A.M., 1992. $^{238}U–^{230}Th–^{226}Ra$ disequilibrium in young Mt. Shasta andesites and dacites. Journal of Volcanological and Geothermal Research 53, 227–238.

Volpe, A.M., Goldstein, S.J., 1993. $^{226}U–^{230}Th$ disequilibrium in axial and off-axis mid-ocean ridge basalts. Geochimica Cosmochimica Acta 57, 1233–1241.

Wagner, G.A., 1998. Age Determinations of Young Rocks and Artifacts. Springer, Berlin, 350pp.

Williams, R.W., Gill, G.B., Bruland, K.W., 1986. Ra-Th disequilibria systematics: timescale of carbonatite magma formation at Oldoinyo Lengai volcano, Tanzania. Geochimica Cosmochimica Acta 50, 1249–1259.

Williams, R.W., 1987. Igneous geochemistry—reading radioactive rock clocks. Nature 325, 573–574.

Wilson, H.W., 1965. Factors affecting the accuracy of assay. In: Leuiham, J.M., Thomson, S.J. (Eds.), Activation Analysis, Proceedings of a NATO Advanced Study. Institute Glasgow Academic Press, London, pp. 91–96.

Wyssling, G., Eikenberg, J., 2000. The geological evolution of the Hell Grottoes at Baar/Zug, Switzerland. Vierteljahresschrift der Naturforschenden Gesellschaft Zürich 145/1, 13–30 (in German).